平成３０年度

博士後期学位論文

Study on Patients' EEG Analysis and Realization of Online Diagnostic System

患者脳波データの解析及びオンライン診断システムの実現に関する研究

繆　堯

埼玉工業大学大学院　博士後期課程

工学研究科　電子工学専攻

指導教員　曹　建庭　教授

概要

脳波（EEG、electroencephalograph）は脳死判定および癲癇診断重要なツールた。本論文は患者脳波データの解析及びオンライン診断システムの実現に関する研究である。

脳死とは脳幹を含めた全脳の機能が不可逆的に停止した状態と定義されている。脳死の定義に基づいた、多くの国が脳死判定の基準を確立している。日本においては（１）深昏睡である、（２）瞳孔散大、（３）脳幹反射の消失、（４）自発呼吸の消失、（５）平坦脳波の基準で脳死判定を行っている。脳死判定の実施中に、自発呼吸の有無検査のリスクや長い脳死判定時間によるリスクを避けするため、脳波予備検査システムを導入された。本論文では脳波予備検査システムで脳死患者と昏迷患者の脳波のエネルギー特徴を解析する。

経験的モード分解法（EMD、 Empirical Mode Decomposition）と多変量経験的モード分解法(MEMD 、Multivariate Empirical Mode Decomposition)を使用して脳波エネルギーを計算することができる。しかし、EMD を使用してマルチチャネル信号を分析することはできない。また、MEMD はマルチチャネル信号を解析することができるが、解析中に信号を超平面に投影する必要があるため、計算量が増加する。そこで、動的旋回正接経験的モード分解法(2T-EMD、Turning Tangent Empirical Mode Decomposition）を提案した。MEMD と比較して、２T-EMD 分解法は超平面上に信号を投影せずに信号を解析する。これにより、計算量が削減され、実時間システムを実現することに近づく。

本論文では、2T-EMD の最適性を述べるために、EMD、MEMD、２T-EMD をアルゴリズムの原理と実験の両面から比較した。実験では標準的な人工信号と患者の脳波にそれぞれに基づいている。最終結果は、3 つの脳波エネルギー計算アルゴリズムにおける 2T-EMD の最適であることを検証した。次に、動的に患

者の脳波エネルギーを解析するために、動的 2T-EMD（Dynamic 2T-EMD）が提案される。Dynamic 2T-EMD は、時間窓と時間ステップを導入することによって、2T-EMD の動的拡張する。動的２T-EMD 分解法を基づき，脳死患者と昏迷患者の脳エネルギーを積算した。また、記述統計（Descriptive Statistics）の手法を使用し、脳エネルギー特徴の分布などを分析した。これらの結果は、脳死患者より、昏迷患者の脳エネルギー値は高く、昏迷患者の脳エネルギー値分布は分散していることを分った。

癲癇とは脳神経細胞の突然の激しい電気的な興奮によって引き起こされる一過性の脳機能不全の慢性疾患であり、最も頻度が高い神経疾患のひとつである。脳波検査は癲癇診断の中で重要な検査である。今癲癇の臨床診断は基本的に医師自身の臨床経験に基づいており、視覚的検出を用いて連続的な脳波から「癲癇脳波」を見つける。発作の不確実性のために、被験者の長期的な検出が必要である。これは長い手動検出および低い効率のような欠点につながる。したがって、癲癇の診断において癲癇発作の自動検出のための信号処理方法を適用する必要がある。本論文では、位相振幅カップリング（PAC、Phase－Amplitude Coupling）を用いて、癲癇発作を検出した。

PAC とは高周波振幅が低周波位相によって変調されると定義される。ボン（Bonn）脳波データセットに基づいて、発作期脳波と発作間欠期脳波の低周波位相と高周波振幅との間のカップリング特徴を解析した。そして、これらのカップリング特徴をサポートベクターマシン(SVM、Support Vector Machine)を用いて分類した。その後、クロスバリデーションによるレシーバ動作特性（ROC with CV、Receiver Operating Characteristics with Cross―Validation）を用いて分類結果を示す。その結果は、シータ帯域とガンマ帯域の間に発作期間における EEG の強いカップリング強度があることを示した。

上記の研究はオフラインデータに基づいているため、医師に適時の分析基

準を提供することは不便である。本論文では、オンライン診断システムを提案する。オンラインシステムは g.tec のアプリケーションインターフェース(API、Application Interface) に基づいて開発されています。システムはラップトップと脳波記録装置で構成され、開発環境は Matlab に基づいている。開発されたシステムを使用することにより、オンライン分析のために EEG 記録装置からラップトップにオンラインデータストリームを転送することができる。さらに、解析結果が予め設定された閾値よりも大きい場合には、警告機能を追加することで、医師に適時に適切な診療を促すことができる。今後の研究では、脳波を解析してシステムの性能を向上させるためのより効率的なアルゴリズムを開発する予定です。

本論文は５章で構成されている。第 1 章では研究の背景と目的である。第 2 章では、提案する動的 2T-EMD アルゴリズムと、動的 2T-EMD と統計解析手法を用いた結果解析を提案し、脳死判定の脳波解析を行っている。第 3 章では、癲癇発作検出の脳波解析である。そこで、発作検出のために低位相周波数と高振幅周波数の間の結合特性を抽出するために使用された PAC 法を示している。第 4 章では、リアルタイム脳波診断支援システムの実現について述べる。システムの構成および原理について説明している。第 5 章は結論と将来の研究課題である。

Abstract

EEG (electroencephalography) is an important tool for brain death determination and seizure detection. In this thesis, patients' EEG analysis and online diagnostic system are studied.

Brain death is defined as the complete, irreversible and permanent loss of brain and brain-stem functions. Many countries have established the criteria of BDD (brain death determination). The criteria of BDD in Japan includes: (1) deep coma; (2) pupil dilatation; (3) disappearance of brainstem reflex; (4) disappearance of spontaneous breathing; (5) flat EEG. In order to avoid the risks existed in the test of disappearance of spontaneous breathing and the risk caused by long time of brain death determination, the EEG preliminary examination system was introduced. In this thesis, coma and brain-death patients' EEG energy features in EEG preliminary examination system were analyzed.

Both EMD (empirical mode decomposition) and MEMD (multivariate empirical mode decomposition) can be used to compute EEG energy features. But EMD is not capable to process multi-channel signals. And though MEMD can be used to analyze multi-channel signals, computational complexity is increased as it is necessary to project signals onto a hyperplane during analysis. So 2T-EMD (turning tangent empirical mode decomposition) is proposed. Compared with the MEMD, the 2T-EMD method analyzes the signal without projecting the signal on the hyperplane, which reduces the computational complexity. In order to illustrate the optimality of 2T-EMD, the three algorithms EMD, MEMD, and 2T-EMD were compared from algorithm principle and experiment, in which the experiments were based on standard artificial signals and patients' EEG respectively. The final result verifies the

optimality of 2T-EMD in three EEG energy calculation algorithms. Then coma and brain-death patients' EEG energy are computed by using Dynamic 2T-EMD. Hereafter the EEG energy features are analyzed by descriptive statistics to get EEG energy differences between coma patients' EEG and brain-death patients' EEG. Results show that EEG energy in coma state is higher than EEG energy in brain-death. Moreover, the EEG energy distribution is more dispersed.

Epilepsy is a chronic disease, which is transient brain dysfunction caused by the sudden and intense electrical excitement of brain neurons. It is one of the most frequent neurological diseases. EEG examination is important examination in the diagnosis of epilepsy. Currently, the clinical diagnosis of epilepsy is basically based on the doctor's own clinical experience, using visual detection to find "epileptic waves" from continuous EEG. Due to the uncertainty of the seizure, long-term detection of the subject is necessary, which leads to disadvantages such as long manual detection and low efficiency. Therefore it is necessary to apply signal processing methods for automatic detection of epilepsy EEG in the diagnosis of epilepsy. In this thesis, PAC (phase-amplitude coupling) was used to detect seizures.

Phase-amplitude coupling is explained as that the high-frequency amplitude is modulated by the low-frequency phase. Based on the Bonn dataset, the coupling features between the low frequency phase and the high frequency amplitude of EEG in seizures and EEG in seizure-free interval were analyzed. And then these PAC strength features are classified by SVM (support vector machine). Hereafter, the classification results are presented by using ROC with CV (receiver operating curve with cross validation). Results showed that there existed a strong coupling strength of EEG in the seizure period between the theta band and the gamma band.

Since the above studies are based on offline data, it is inconvenient to provide

doctors timely analysis reference. In this paper, the online diagnosis system is proposed. The online system is developed based on API (Application Programming Interface) of g.tec. The system consists of a laptop and an EEG recording device.

Finally, we develop the API (Application Programming Interface) between EEG recording device and EEG analysis software. By using the developed API, online data streams can be transferred from EEG recording device to the EEG analysis software, thereby realize the function of online EEG recording and online EEG analysis. Furthermore, a warning function is added when the analysis result is larger than a preset threshold value, which can remind the doctor timely to take appropriate medical treatment to the patient. In future research more efficient algorithms to analyze EEG will be developed and the system performance will be improved.

Specifically, the thesis is divided into five Chapters. Chapter 1 is the research background and purpose. Chapter 2 is the EEG analysis for brain death determination. This chapter illustrates the proposed Dynamic 2T-EMD algorithm, and the results analyzed by using Dynamic 2T-EMD and statistical analysis method. Chapter 3 is the EEG analysis for seizure detection. This chapter illustrates PAC method was used to extract coupling features between low phase frequency and high amplitude frequency for seizure detection. Chapter 4 is the realization of online EEG diagnostic system. This chapter illustrates the composition and realization of the system. Chapter 5 is the conclusions and future work.

Acknowledgement

My sincere and deep gratitude goes first and foremost to my supervisor, Prof. Jianting Cao, for his careful guidance, valuable suggestions, great patience and constant encouragement throughout my study. And I would like to express my sincere appreciate for the valuable study opportunities and support provided by Prof. Jianting Cao.

I would like to express my sincere gratitude to Prof. Toshihisa Tanaka in Tokyo University of Agriculture and Technology, for his valuable guidance on data analysis methodology.

I would like to express my sincere appreciate to Saitama Institute of Technology and Hangzhou Dianzi University for the sponsorship of the international exchange program.

I would like to express my sincere gratitude to Vice President/ Prof. Dongying Ju for providing me the valuable opportunity of studying in Japan and ongoing help.

I would like to express my sincere thanks to Prof. Yoshizawa, Prof. Watabe, Prof. Yamasaki and Dr. Qibin Zhao in RIKEN Center for Advanced Intelligence Project for sparing time out of their busy schedules in reviewing my dissertation and giving precious comments in revising the thesis.

I would like to express my sincere appreciation to researchers I met in Brain Science Institute, RIKEN for their valuable guidance and help.

I would like to thank students and teachers I met in Saitama Institute of Technology for their help.

At last but not least, I would like to express my heartfelt gratitude to my beloved parents and elder brother for their encouragement and support. I am really indebted to them.

Table of Contents

Chapter 1 Introduction

1.1 Background of Coma and Brain-Death EEG Analysis

The concept of brain death was first proposed by Mollaret and Goulon in 1959 and then constantly being corrected [1]. In 1968, the Ad Hoc Committee of the Harvard Medical School to Examine the Definition of Brain Death proposed the definition of irreversible of coma, also known as the Harvard criteria, which is the first diagnostic criteria of brain death in human history [2]. From then on, there is a strict definition of brain death in medicine and law, which is the complete, irreversible and permanent loss of brain and brain-stem functions. Hereafter, many countries have established the determination criteria of brain death based on the definition [3]. For example，the criteria of brain death determination in Japan is as shown below.

(1) Coma test.

(2) Pupils test. Both sides of pupils dilate more than 4mm and pupils fixation.

(3) Brainstem reflexes test. It includes the test of pupils light reflection, corneal reflex, ciliary spinal reflex, oculocephalic reflex, vestibular reflex, swallow reflex and cough reflex.

(4) Apnea test. The patients lost spontaneous breathing function without connecting the ventilator.

(5) EEG confirmatory test. There is no EEG higher than $2\mu V$.

The above steps are needed to check twice, and the interval of duration between the two checks is not less than 6 hours.

So there may exist two risks in the above mentioned criteria of brain death determination. One risk is that it takes long time of the checks since the EEG recording required for 30 minutes and the interval of duration between the two checks

is more than 6 hours. The other risk exists in apnea test as the apnea test requires close monitoring of the patient under the circumstance that all ventilator support is temporarily removed and $PaCO_2$ (Pressure of carbondioxide) levels are allowed to rise [4]. Based on the risks explained above, an EEG preliminary examination system between the brainstem reflex test and apnea test for the brain death determination was introduced [5]. The establishment of this preliminary system is helpful to reduce clinical risk and prevent clinical misjudgment.

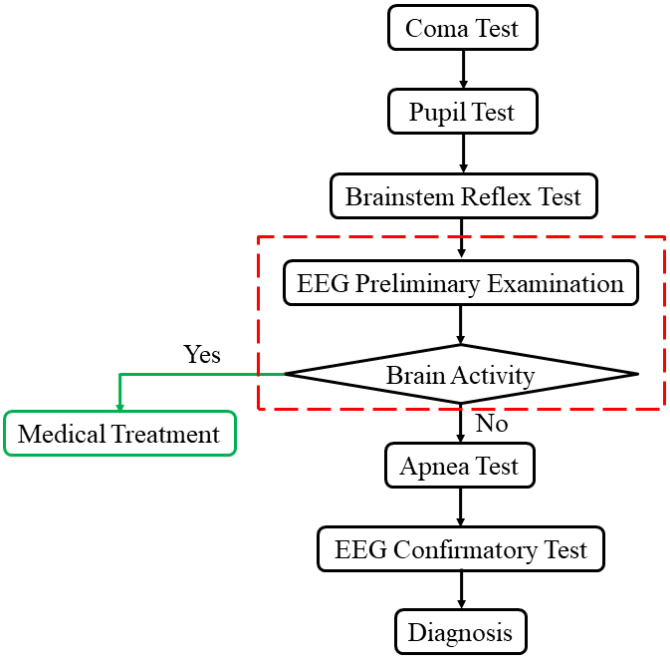

Fig. 1.1 Procedures of EEG preliminary examination based on brain death determination.

The procedure of EEG preliminary examination based on brain death determination is described in figure 1.1. In details, in the procedures of EEG preliminary examination, patients in quasi-brain-death state are conducted coma test, pupil test and brainstem reflex test firstly. Then the procedure of EEG preliminary examination is introduced to evaluate whether the patient has an obvious rhythmic EEG. If exists, the procedures stop and further medical assistance is provided timely to the patient according to the patient's condition. On the contrary, if there is no brain activity, the procedures of brain death determination are conducted continuously. So in order to provide the accurate preliminary diagnosis in the EEG preliminary examination, it is

necessary to develop advanced EEG signal processing algorithms. This is also the purpose of the first part in the thesis.

Several EEG analysis algorithms were applied to analyze quasi-brain-death state patients' EEG by extracting different features such as energy and complexity. In this thesis, we mainly focus on the algorithms development based on EEG energy features. EMD-based algorithms, as fully data driven algorithms, can be used to analyze nonlinear and nonstationary signals and compute EEG energy of signal at any time to avoid the loss of signal information. In related work, EMD was applied to process quasi-brain-death patients' EEG and good results were obtained in terms of EEG energy to distinguish between coma and brain death [6]. But EMD can't be used to analyze multivariate EEG signals. So MEMD was introduced [7]. Dynamic MEMD was proposed as it was difficult to display the EEG energy fluctuation over time for the results analyzed by static EMD-based results [8]. However, it was needed to project the multivariate signals to the hyperplane for Dynamic MEMD algorithm, which resulted in a large amount of computation.

Therefore, in this thesis, the Dynamic 2T-EMD algorithm is proposed to process multi-channel coma and brain-death patients' EEG, where no signal projection is required. Firstly, the dataset used in this part were illustrated. Secondly, principles of three static EMD-based (EMD, MEMD, 2T-EMD) algorithms were compared as well as the Dynamic 2T-EMD algorithm was explained. Thirdly, experiments for three static EMD-based algorithms were conducted to verify the optimal performance of 2T-EMD from experimental perspective, where the experiments were based on standard artificial signals and patients' EEG. Moreover, EEG energy of 36 cases of coma and brain-death patients' EEG were computed by Dynamic 2T-EMD from overall aspect. At the same time, two typical patients' EEG who were in coma state

and brain-death state respectively as well as one special patient's EEG who was from coma to brain-death were also analyzed by Dynamic 2T-EMD to obtain EEG energy features from individual aspect. Finally, the EEG energy features were analyzed by descriptive statistical method. Final results showed that there existed significant differences of EEG energy between coma EEG and brain-death EEG. In detail, the EEG energy in coma state was higher than EEG energy in brain-death state, and the EEG energy distribution of coma patients' EEG was more dispersed than that of brain-death patients' EEG.

1.2 Background of Epilepsy EEG Analysis

The International League Against Epilepsy (ILAE) formulated conceptual definitions of seizure and epilepsy in 2005, that is, an epileptic seizure is defined as a transient occurrence of signs and/or symptoms due to abnormal excessive or synchronous neuronal activity in the brain by the International League Against Epilepsy (ILAE), as well as epilepsy is a disorder of the brain characterized by an enduring predisposition to generate epileptic seizures, and by the neurobiological, cognitive, psychological, and social consequences of this condition. Moreover, the definition of epilepsy requires the occurrence of at least one epilepsy seizure [9]. Epilepsy is a common complex spectrum disorder that can affect individuals of all ages [10]. Approximately 50 million people worldwide have epilepsy, making it the most common neurological disease globally [11, 12]. Epilepsy is characterized by unpredictable seizures, which influence the quality of life for patients and their families. Long-term anti-epileptic drugs therapy is the one form of treatment, up to 70% of people could have their seizures fully controlled with appropriate drugs therapy [13, 14]. For patients of drug-resistance epilepsy, epilepsy surgery is the primary treatment [15, 16]. Around 70% of people (7 in 10 people) who have

temporal lobe surgery find that the surgery stops their seizures [17]. The success of epilepsy surgery is directly related the location and resect or disconnect accurately the epileptogenic cortex [18]. There are some tools to be used currently in the location and characterization of seizures, such as single photon emission computed tomography/position emission tomography scans, magnetic resonance imaging, surface or and intracranial EEG recordings [19]. Computed tomography can cause damage to the human body. And the cost of magnetic resonance imaging is high, which may cause economic burden for patient. Compared with computed tomography and magnetic resonance imaging, EEG is the primary diagnostic tool for epilepsy because it is harmless to human body with low cost. In this paper, we mainly focus on EEG recordings.

EEG recordings are time-varied non-stationary signals, which are mainly composed by basic elements of frequency, amplitude and phase. Currently the clinical diagnosis of epilepsy is basically based on the doctor's clinical experience by visually observing the patient's EEG. In details, the EEG of a patient with epilepsy appears interictal epileptiform discharges, such as EEG spike and EEG sharp waves, which were well-recognized hallmarks of epilepsy [20]. However due to the predictable of the seizure, long-term detection of the subject is necessary. But this leads to a large amount of EEG data, which leads to disadvantages such as long manual detection and low efficiency for doctors. In addition, due to the large individual differences in seizures, doctors are susceptible to subjective factors when diagnose by visually observing EEG. Moreover, some important features of the seizures are difficult to observe directly from the EEG, such as high-frequency oscillation characteristics and coupling characteristics of EEG. Therefore it is necessary to apply signal processing methods for automatic detection of epilepsy EEG in the diagnosis of epilepsy. It will

improve detection efficiency and reduce the work pressure for doctors. In this thesis, PAC (phase-amplitude coupling) was used to detect coupling features of seizures.

Phase-amplitude coupling, one type of cross-frequency coupling (CFC), is a common method used for analysis of EEG analysis, as it reveals the coupling on high-frequency amplitude modulated by low-frequency phase. Some studies have shown that coupling is closely related to brain activity. For example, Coupling of high frequency oscillation and low frequency oscillation was an important basis for completing brain function [21]. And the cross-frequency coupling between theta band and gamma band has improved working memory performance [22]. And many studies have shown the differences of coupling between epilepsy zone and normal zone. For example, research has shown that the phase-amplitude coupling was elevated in the seizure-onset zone for the children with medically-intractable epilepsy secondary to focal cortical dysplasia [23]. And delta-modulated high-frequency oscillation may provide accurate localization of epileptogenic zone by identifying the regions of interest for extratemporal lobe patients [24]. Moreover, the phase-amplitude coupling in seizure onset zone was higher than normal zone [25]. Furthermore, the cross-frequency coupling information can be used to locate the epileptogenic zone [26]. In this thesis, in order to identify EEG of seizure activity and EEG of seizure-free interval, 5 methods of computing PAC features were introduced to analyze the coupling features between low frequency phase and high frequency amplitude. Specifically, phase-amplitude coupling features between different low frequency oscillation and high frequency oscillation were extracted respectively by 5 PAC methods. And based on extracted coupling features, the EEG of seizures activity and EEG of seizure-free intervals were classified by using support vector machine. Afterward, the classification results were evaluated by introducing receiver operating

characteristics with k-fold cross-validation. Final results showed that there existed obvious coupling features between θ band phase and γ band amplitude for EEG in seizures, with the classification result was up to 0.99 for the EEG of seizures within epileptogenic zone and the EEG of seizure-free intervals not in epileptogenic zone. And the results analyzed by 5 different methods of computing PAC were close.

1.3 Thesis Outlines

In this thesis, we mainly study on the patients' EEG analysis and propose an online EEG diagnostic system. Specifically, there are three parts of content, coma and brain-death patients' EEG analysis by using newly proposed Dynamic 2T-EMD algorithm, epilepsy EEG analysis by applying 5 methods of computing PAC, and the realization of online EEG diagnostic system. The outlines of this thesis are organized as below.

Chapter 1 illustrates the background of coma and brain-death patients' EEG analysis as well as the background of epilepsy EEG analysis. Firstly, this chapter explains the definition of brain death, the criteria of brain death determination, and the procedures of EEG preliminary examinations based on brain death determination firstly. And it illustrates current research methods of coma and brain-death patients' EEG analysis based on EEG energy features. Then based on the insufficient of existed algorithms for extracting EEG energy features in coma and brain-death state, the first research content is proposed of this thesis. Secondly, in this chapter, the definition and research significance of epilepsy, as well as the current research progress of epilepsy EEG analysis based on phase-amplitude coupling are briefly clarified. Then in order to detect accurately features of phase-amplitude coupling in seizure activity, the second research content is proposed of this thesis.

Chapter 2 introduces firstly dataset used in this chapter and three static EEG-based

algorithms, and compares the three algorithms to get the optimal static algorithm based on principle and experiments, in which experiments are based on standard artificial signals and patients' EEG respectively. Then Dynamic 2T-EMD is newly proposed based on optimal performance of static 2T-EMD. Hereafter, 36 cases of coma and brain-death patients' EEG are processed by Dynamic 2T-EMD, and the results are analyzed by descriptive statistics from 3 group measures. Overall results show that there is significant different of EEG energy between coma patients' EEG and brain-death patients' EEG.

Chapter 3 describes epilepsy EEG dataset used in this chapter and five algorithms of computing phase-amplitude coupling strength firstly. Soon afterwards, the epilepsy EEG dataset are processed by five methods of PAC at 9 frequency bands to extract PAC strength features respectively. And these PAC strength features are classified by using support vector machine according to different PAC computing method and different bands in order to obtain the coupling features of seizure activity. The classification performance is presented by using *k*-fold ROC based Cross-Validations. Furthermore, phase-amplitude comodulograms measures based on five PAC methods are used to provide visual verification of classification results. Results show that there exists obvious phase-amplitude coupling strength in EEG during seizure activity at $\theta - \gamma$ band, and the classification results is up to 0.96 at band $\theta - \gamma$ within epileptogenic zone. Results also show that the accuracy is 0.99 for classify seizure-free intervals not in epileptogenic zone and seizures within epileptogenic zone.

Chapter 4 illustrates the realization of online EEG diagnostic system. This chapter explains the composition and framework of the system. And the experiment based on online calibration signals is described. Results show that the system can realize the

function of online recording and online analysis based on existing algorithms. Furthermore, the system can also realize the alarm function when the analysis results higher than the preset threshold.

Chapter 5 states the conclusion and future work based the existing content in this thesis. For coma and brain-death EEG analysis, the Dynamic 2T-EMD algorithm is proposed and used. It is show that compared with brain-death patients' EEG, the EEG energy of coma patients' EEG is obvious higher. For epilepsy patients' EEG analysis, the five methods of computing PAC strength as well as support machine vector are used to process epilepsy EEG during seizure activity and seizure-free intervals. From the classification results, there exists stronger coupling strength at $\theta - \gamma$ for patients' EEG of seizure activity. The comodulogram results verify the classification results. The above contents are based on offline patients' EEG, so an online EEG diagnostic system is proposed in order to realize the combination of online recording and online analysis based on existed algorithms. In future work, deep learning methods will be applied in classification of quasi-brain-death patients' EEG as well as the detection of seizure. Moreover, the function of system will be optimized from interactive interface and stability.

1.4 Chapter Summary

This chapter illustrates the background of coma and brain-death patients' EEG analysis, epilepsy patients' EEG analysis and the realization of online EEG diagnostic system. In addition, the chapter describes the structure of the thesis.

Chapter 2 Coma and Brain-Death EEG Analysis

2.1 Materials

2.1.1 Standard Artificial Signals

Since the frequency of coma and brain-death EEG was lower than 40Hz, 80 sets of standard artificial signals were selected to test the computational performance of 3 static EMD-based algorithms. Each of standard artificial signals was composed of a low frequency sinusoidal signal of each different frequency and the high frequency sinusoidal signal of 100 Hz, in which the frequency range of the low frequency sinusoid signals was 0~40Hz and the interval frequency was 0.5Hz. Take a simple example shown in figure. 2.1.

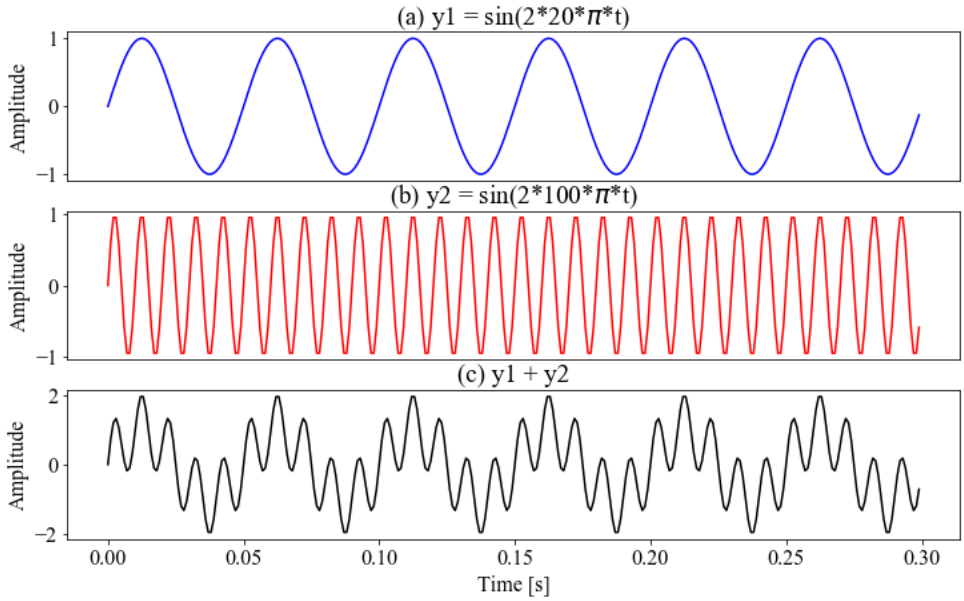

Fig. 2.1 Standard artificial signals. (a) was the low frequency sinusoidal signal of 20Hz, (b) was the high frequency sinusoidal signal of 100 Hz, (c) was the standard artificial signals composed by (a) and (b).

2.1.2 Coma and Brain-Death EEG

The EEG data we used in the paper were recorded in EEG preliminary examination in a Chinese hospital from June 2004 to March 2006, with the permission of patients'

families [27]. During the EEG recording, patient was lying on the bed in the ICU. And the EEG data was detected by the portable NEUROSCAN ESI-64 system and a laptop computer. Six exploring electrodes (Fp1, Fp2, F3, F4, F7, F8) as well as one ground electrode (GND) were placed on the forehead, and two reference electrodes (A1, A2) were placed on earlobes. And the sampling frequency was 1000Hz and the electrode resistance was lower than 8KΩ. The placement of electrodes was shown in figure. 2.2. In this paper, the EEG of 35 coma and quasi-brain-death patients (male:21; female:14) with a total of 36 cases of EEG (coma:19; quasi-brain-death:17), in which there were one case of EEG in coma and one case of EEG in quasi-brain-death included in the same special patient whose state was from coma state in the first EEG recording process to quasi-brain-death state in the second EEG recording process after about 10 hours.

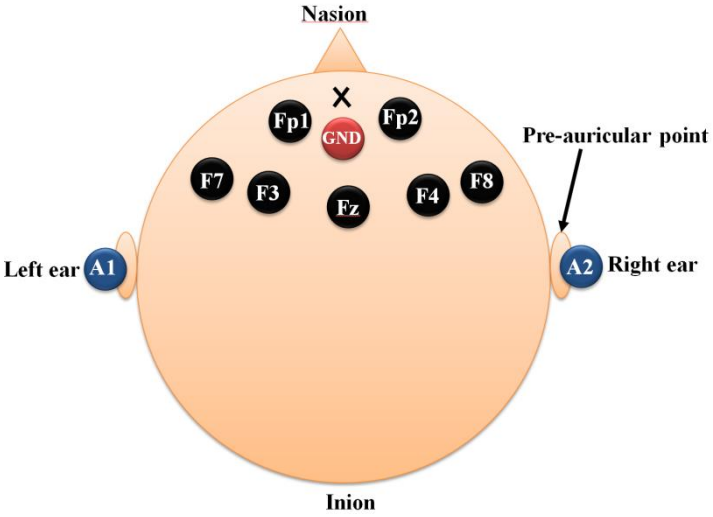

Fig. 2.2 The placement of 9 electrodes.

2.2 Energy Feature Extraction Methods

2.2.1 Static EMD-Based Algorithms

Static EMD-based algorithms, EMD, MEMD and 2T-EMD are fully data-driven algorithms for multiscale decomposition and time-frequency analysis of real-valued signals [28]. The principle of the three algorithms has in common in that, the complex,

non-linear and non-stationary signal is decomposed into a finite set of IMFs (Intrinsic Mode Functions) and a monotonic residual signal based on local time feature scale of signal. As shown in figure 2.3. Here the IMF must satisfy two conditions, one is the number of zero crossing and the number of extrema differing at most by one, and the other is that the upper and lower envelopes of the signal are symmetrical.

As described in formula (2-1), for a real-valued signal $x(t)$, the algorithm principle of EMD is to decompose $x(t)$ into a finite set of IMFs $\sum_{n=1}^{n=N} IMF_n$ and a monotonic residual signal $r(t)$.

$$x(t) = \sum_{n=1}^{n=N} IMF_n + r(t) \tag{2-1}$$

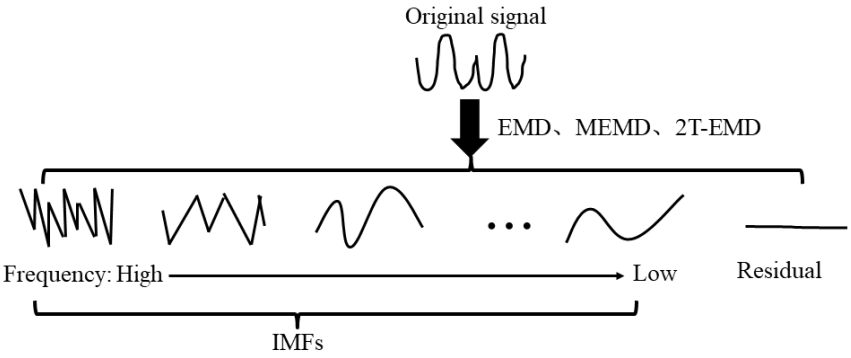

Fig. 2.3 Basic Schematic of static EMD-based algorithms.

The principle flow chart of EMD is shown in figure 2.4. The key of EMD algorithm is the computation of local mean of the original signal, which is computed by taking the average of upper envelopes and lower envelopes. The envelope is obtained by connecting all local extrema through using cubic spline line. Specifically, for a single channel signal $x(t)$, extract all local maximum $x_{l_{max}}$ and all local minimum $x_{l_{min}}$, and connect all $x_{l_{max}}$ and $x_{l_{min}}$ by using cubic spline line respectively to get the upper envelope $L_{max}(t)$ and lower envelope $L_{min}(t)$. Then take mean of $L_{max}(t)$ and $L_{min}(t)$.

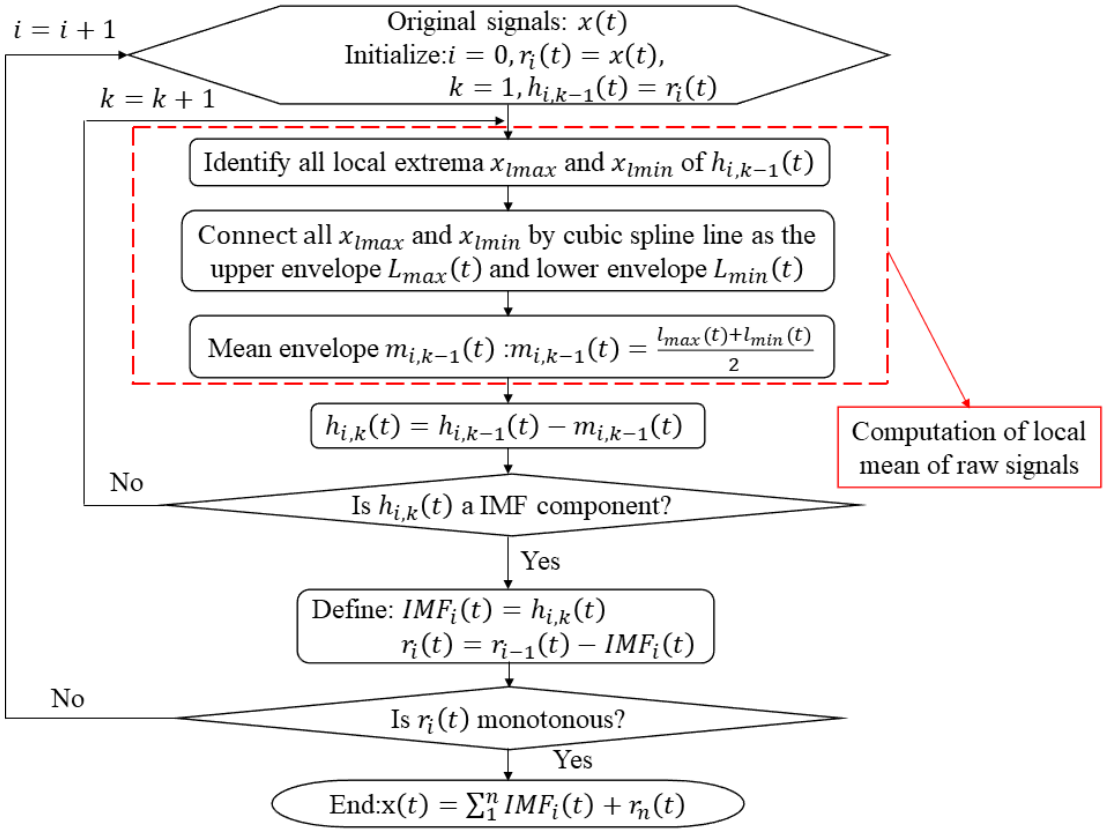

Fig. 2.4 The principle flow chart of EMD.

But for multivariate signals, the local extrema may not be defined directly. The MEMD algorithm solved this problem by taking signal projections along different directions in *n*-dimensional spaces, and these signal projections are then averaged to obtain the local mean. More specifically, for a multivariate signal with *n* components $\{\vec{v}(t)\}_{t=1}^{T} = \{v_1(t), v_2(t), \cdots v_n(t)\}_{t=1}^{T}$ which is a sequence of *n*-dimensional vectors, and a set of direction vectors $\{\vec{x}^{\theta_k}\}_{k=1}^{K} = \{x^{\theta_1}, x^{\theta_2}, \cdots, x^{\theta_K}\}$ that are along the directions given by angels $\{\vec{\theta}_k\}_{k=1}^{K} = \{\theta_1, \theta_2, \cdots \theta_K\}$ on a $(n-1)$ sphere, the computation of local mean of MEMD algorithm is shown in figure 2.5 [29].

Although the MEMD algorithm can be used to decompose multivariate signals, with using real-valued projections along multiple directions on hyperspheres in order to calculate the local mean of the multivariate signals, which may result in a large amount of computation.

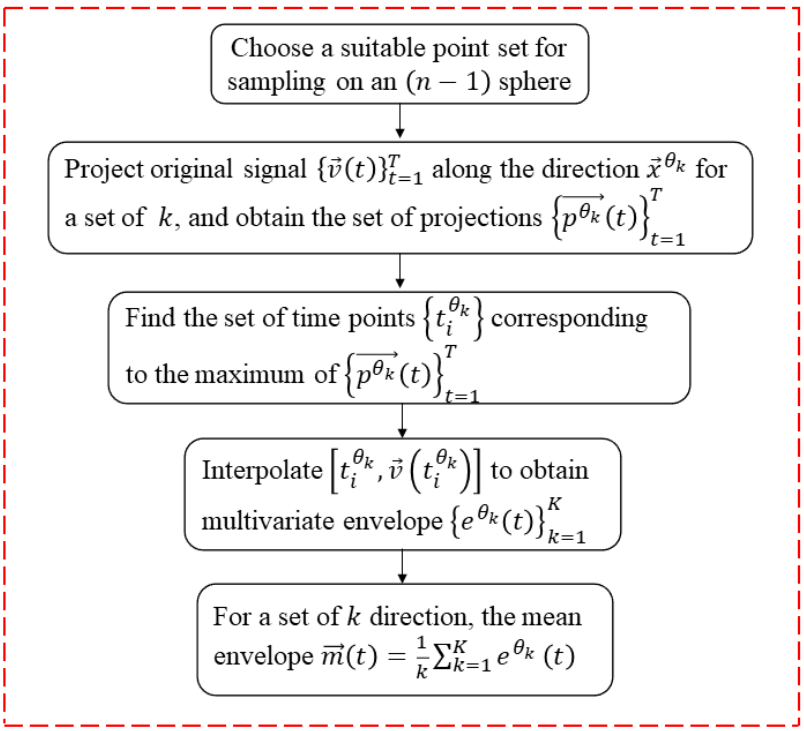

Fig. 2.5 Flow chart of the computation of local mean for MEMD.

The 2T-EMD offers the possibility to decompose multi-channel signals without projections by redefining and computing the signal mean envelope, and the re-definition of the signal mean trend, which is obtained by interpolating between barycenter of particular oscillation, or called elementary oscillation. Specifically, the key of 2T-EMD is the computation of signal mean trend, which is obtained by averaging two envelopes: a first envelope interpolates the even indexed barycenters which include signal borders, and a second envelope interpolates the odd indexed barycenters which also include signal borders [30]. Moreover, the 2T-EMD can process single and multi-channel signals. Let s be a class C^1 function in R^D domain and differentiable with a continuous first derivative. The sifting procedure of computing the signal mean trend is briefly illustrated as Algorithm (1) [31]. And the computation flow chart of local mean of 2T-EMD is shown in figure 2.6.

Algorithm 1 2T-EMD Algorithm

1. Defined a time series $\vec{T}(s)$ as the tangent vector to s and express as:

$$\vec{T}(s): t \to \left[1, \frac{ds}{dt}(t)\right]$$

2. Defined α_s as the Euclidean inner products of R^{D+1} and express as:

$$\alpha_s: t \to \lim_{h \to 0} \langle \vec{T}_s(t-h), \vec{T}_s(t+h) \rangle$$

Due to the continuity of Euclidean inner product, so α_s can be expressed as:

$$\forall t \in R, \alpha_s(t) = \lim_{h \to 0} \langle \vec{T}_s(t-h), \vec{T}_s(t+h) \rangle$$

3. Since s is a class C^1 function, we can get the formula below:

$$\forall t \in R, \qquad \alpha_s(t) = \left\| \vec{T}_s(t) \right\|^2 = 1 + \left\| \frac{ds}{dt}(t) \right\|^2$$

Where $\|\cdot\|$ refers to the Euclidean norm of both R^D and R^{D+1}.

4. Oscillation extremum of function $s(t)$ is defined as below:

$$\beta_s(t): t \to \beta_s(t) = \left\| \frac{ds}{dt}(t) \right\|^2$$

5. Take two consecutive oscillation extrema, respectively $P_1 = [t_1, s(t_1)]^T$ and $P_2 = [t_2, s(t_2)]^T$, thereby $M_{P_1 - P_2}$, the barycenter of the associated elementary oscillation is defined as below:

$$M_{P_1 - P_2} = \left[\frac{t_1 + t_2}{2}, \frac{1}{t_1 - t_2} \int_{t_2}^{t_1} s(t) dt \right]^T$$

6. The mean vector $\vec{e}(t)$ of signal can be obtained according to the definition.

In conclusion, there are two aspects of principle differences among EMD, MEMD, and 2T-EMD, respectively the number of channels analyzed and the computation method of local mean of original signals. The comparison of EMD, MEMD, and 2T-EMD based on algorithm principle is shown in Table 2-1.

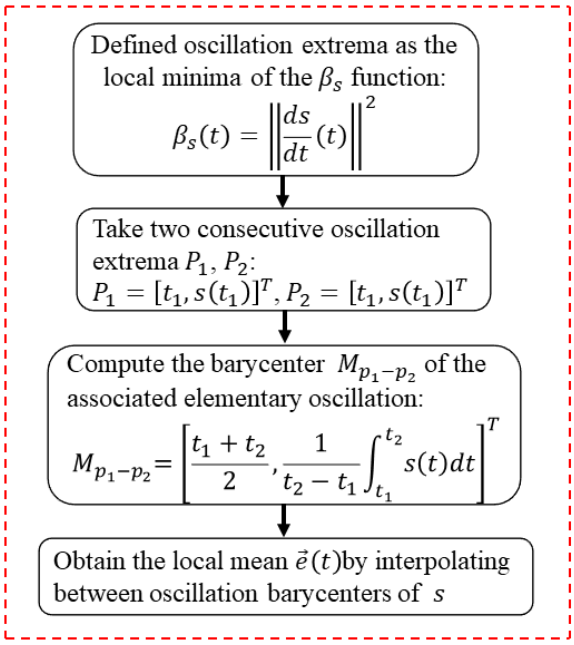

Fig. 2.6 Flow chart of the computation of local mean for 2T-EMD.

Table 2-1 Algorithm Principle Comparison among EMD, MEMD, and 2T-EMD

Method	**Similarity**	**Differences**	
		Type of signal	**Computation method of local mean**
EMD	Original signal $\boldsymbol{s(t)}$ ↓ $\sum_{i=1}^{n} \boldsymbol{IMF_i} + \boldsymbol{r(t)}$ ($\boldsymbol{r(t)}$ is residual)	Single channel	The local mean is calculated as the half sum of the upper and the lower envelopes, obtained by interpolating between local minima and maxima using cubic splines.
MEMD		Multi-channel	Take signal projections along different directions in n-dimensional spaces, and averaged corresponding projections to obtain the local mean.
2T-EMD		Single channel and multi-channel	Identify all elementary oscillations, compute the barycenter of each associated elementary oscillations, and interpolate between all these barycenters to calculate the signal mean trend.

2.2.2 Dynamic 2T-EMD

In order to observe dynamic changes of EEG energy and reduce the influence by noise, Dynamic 2T-EMD is developed by extending 2T-EMD with excellent static EEG energy computational performance. As is shown in figure 2.7, a time window that the width is Δt and a time step with the width $\Delta\lambda$ are introduced in the Dynamic 2T-EMD algorithm, where Δt and $\Delta\lambda$ are controllable parameters. With the time window sliding along the time axis in a time step, a time step of EEG is processed and value is stored. Then steps above are repeated to get the dynamic EEG energy features [32].

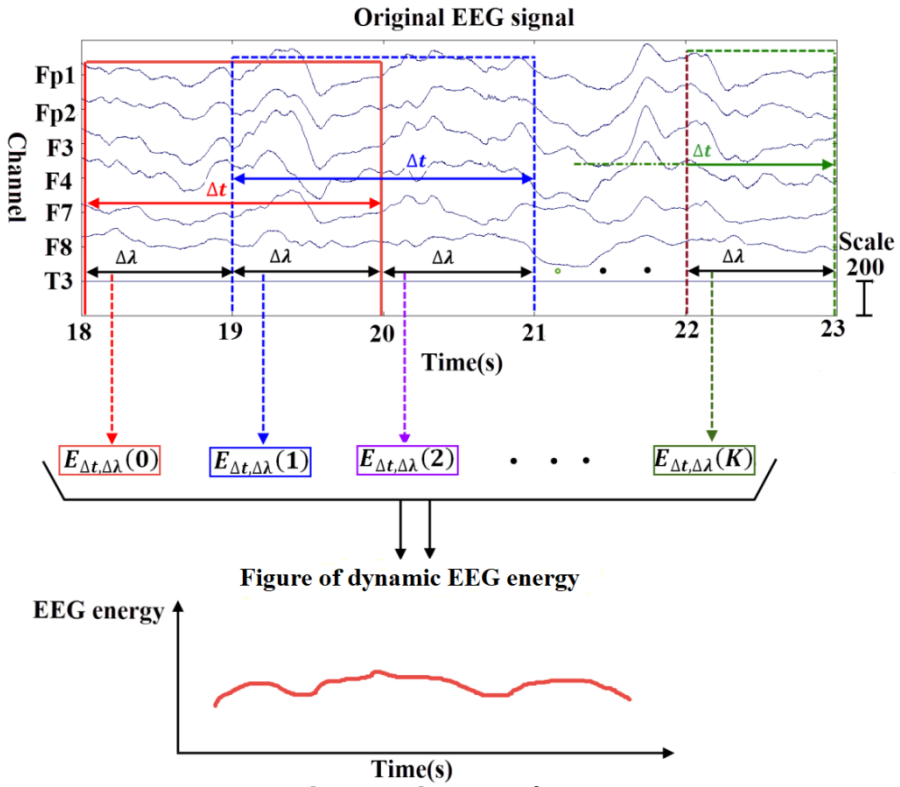

Fig. 2.7 Schematic diagram of Dynamic 2T-EMD

More specifically, for a multivariate signal with n components $\{\vec{s}(k\cdot\Delta t)\}_{k=0}^{K}=\{\vec{s}(0\cdot\Delta t),\vec{s}(1\cdot\Delta t),\cdots,\vec{s}(K\cdot\Delta t)\}$ from T_1 to T_2, where $T_2=T_1+K\cdot\Delta t$. The analysis process of Dynamic 2T-EMD is as shown in Algorithm (2).

Algorithm 2 Dynamic 2T-EMD Algorithm

1. Initialize the number of iteration $j = 1$, the number of IMF $i = 1$,, and the number of time step $k = 0$; and set $\vec{r}_i(k \cdot \Delta t) = \{\vec{s}(k \cdot \Delta t)\}_{k=0}^{K}$, $\vec{h}_{i,j-1}(k \cdot \Delta t) = \vec{r}_i(k \cdot \Delta t)$.
2. Compute the barycenter $M_{(i,j-1)_{P_{k_x}-P_{k_{x+1}}}}(k \cdot \Delta t)$ of random consecutive oscillation extrema P_{k_x} and $P_{k_{x+1}}$ in the period of $k \cdot \Delta t$, that is $M_{(i,j-1)_{P_{k_x}-P_{k_{x+1}}}}(k \cdot \Delta t) = \left[\frac{k_x \cdot \Delta t + k_{x+1} \cdot \Delta t}{2}, \frac{1}{k_x \cdot \Delta t - k_{x+1} \cdot \Delta t} \int_{k_{x+1} \cdot \Delta t}^{k_x \cdot \Delta t} \vec{h}_{i,j-1}(t) dt\right]^T$.
3. Obtain the signal mean trend $\vec{e}_{i,j-1}(k \cdot \Delta t)$ by interpolating between oscillation barycenters of $\vec{h}_{i,j-1}(k \cdot \Delta t)$.
4. Subtract $\vec{\mathrm{e}}_{\mathrm{i,j-1}}(\mathrm{k} \cdot \Delta \mathrm{t})$ from the given signals $\vec{h}_{i,j-1}(k \cdot \Delta t)$, we define $\vec{h}_{i,j}(k \cdot \Delta t) = \vec{h}_{i,j-1}(k \cdot \Delta t) - \vec{e}_{i,j-1}(k \cdot \Delta t)$. If $\vec{h}_{i,j}(k \cdot \Delta t)$ obey the sifting stop criteria, define $\overrightarrow{IMF_i}(k \cdot \Delta t) = \vec{h}_{i,j}(k \cdot \Delta t)$, otherwise repeat the iteration steps from (2) to (4). It is worth noting that the stop criteria is using the Cauchy-like criteria, more precisely, let $d_{i,j}$ be the $i-th$ IMF computed at the $j-th$ iteration of the sifting process, then the sifting criteria is for instance 90% of values $\left\|\frac{d_{i,j+1}(t)-d_{i,j}(t)}{d_{i,j}(t)}\right\|$ are lower than 10-2.
5. Define $\vec{r}_i(k \cdot \Delta t) = \vec{r}_i(k \cdot \Delta t) - \overrightarrow{IMF_i}(k \cdot \Delta t)$, if the result signal is monotonous, we can get the decomposition results of signals during $k \cdot \Delta t$, that is $\vec{s}(k \cdot \Delta t) = \sum_{i=1}^{N} \overrightarrow{IMF_i}(k \cdot \Delta t) + \vec{r}_N(k \cdot \Delta t)$, otherwise repeat steps from (2) to (5).
6. Determine whether the elapsed time $k \cdot \Delta t$ exceeds the end time T_2, if it does, the process goes to end and the final decomposition result $\{\vec{s}(k \cdot \Delta t)\}_{k=0}^{K} = \left\{\sum_{i=1}^{N} \overrightarrow{IMF_i}(k \cdot \Delta t) + \vec{r}_N(k \cdot \Delta t)\right\}_{k=0}^{K}$; If it doesn't, moving the time window and repeat steps from step2 to step 6.

2.3 Results

2.3.1 Results of Comparison among 3 Static EMD-Based Algorithms

In this section, EMD, MEMD and 2T-EMD were compared from experimental aspect based on standard artificial signals and coma and brain-death patients' EEG respectively, in which signal representation accuracy and computational time were compared for standard artificial signals as well as computational time was compared based on coma and brain-death patients' EEG. Here signal representation accuracy was denoted by root-mean-square error (RMSE), shown as formula (2-2). RMSE was used to measure the deviation of processed value and original value, where N is sampling frequency, x_i is the amplitude of artificial signals after processing by algorithms, o_i is the amplitude of original standard artificial signals.

$$\mathrm{RMSE} = \sqrt{\frac{1}{N}\sum_{i=1}^{N}(x_i - o_i)^2} \tag{2-2}$$

A. Results Based on Standard Artificial Signals

The first part is that EMD, MEMD and 2T-EMD were compared based on standard artificial signals. From the content explained in section 2.2.1, we know that EMD algorithm and MEMD algorithm can only be used to process single channel signals and multi-channel signals respectively, while 2T-EMD can process both single and multi-channel signals. So comparison between EMD and 2T-EMD based on single channel standard artificial signals, and comparison between MEMD and 2T-EMD based on multi-channel standard artificial signals were illustrated respectively.

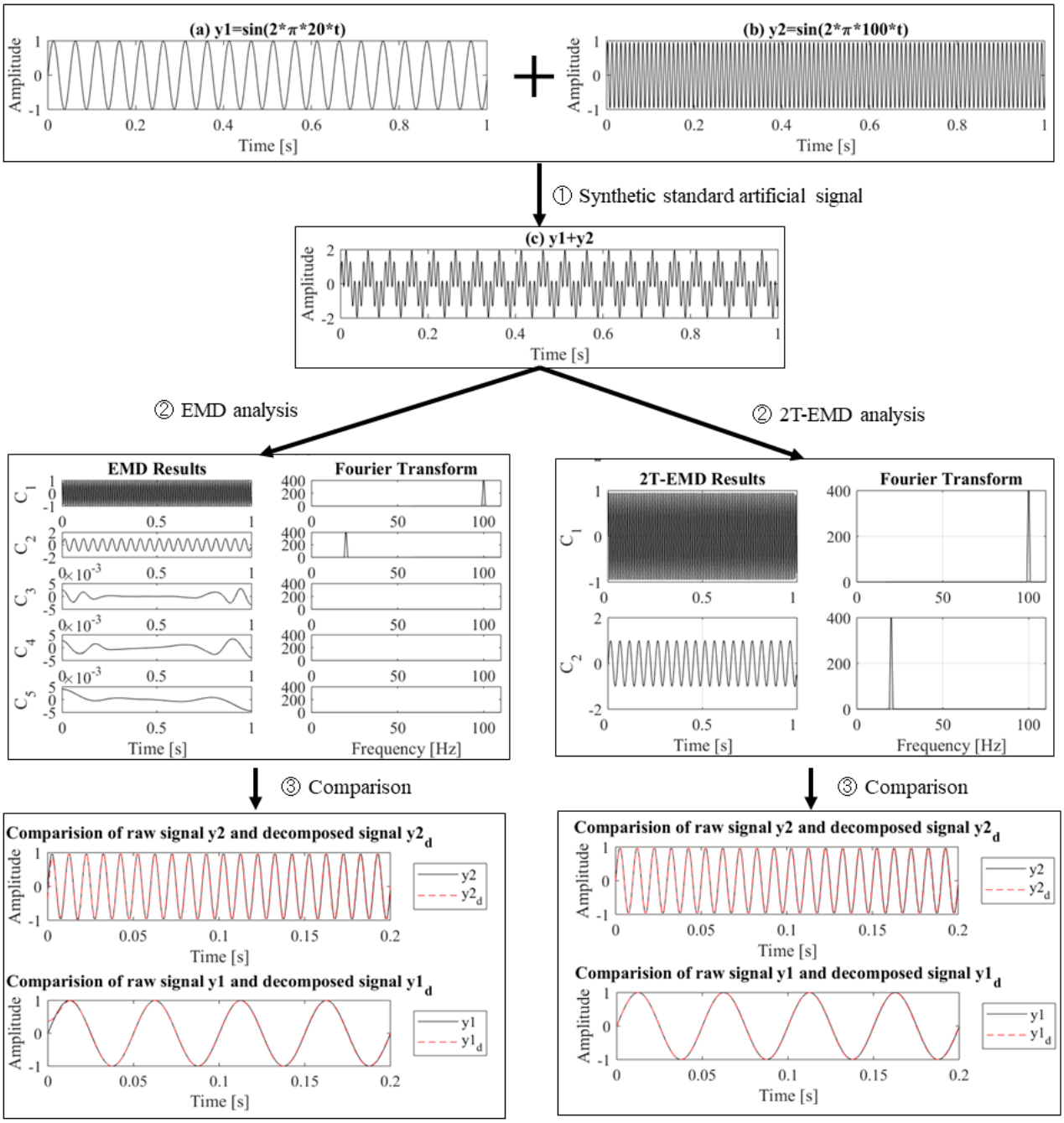

Fig. 2.8 Analysis process of EMD and 2T-EMD based on single channel standard artificial signals. The upper panel ① was the synthesis process of two sinusoid signals $y1 = sin(2 * \pi * 20 * t)$ and $y2 = sin(2 * \pi * 100 * t)$; the middle panel ② was the decomposition process of EMD, 2T-EMD and their corresponding Fourier Transform process; the lower panel ③ was the comparison of raw signals and decomposed signals.

Firstly, EMD and 2T-EMD were used to process the 80 sets of standard artificial

signals explained in section 2.1.1. As shown in figure 2.8 was a simple example to explain intuitively the analysis process of EMD and 2T-EMD based on standard artificial signals.

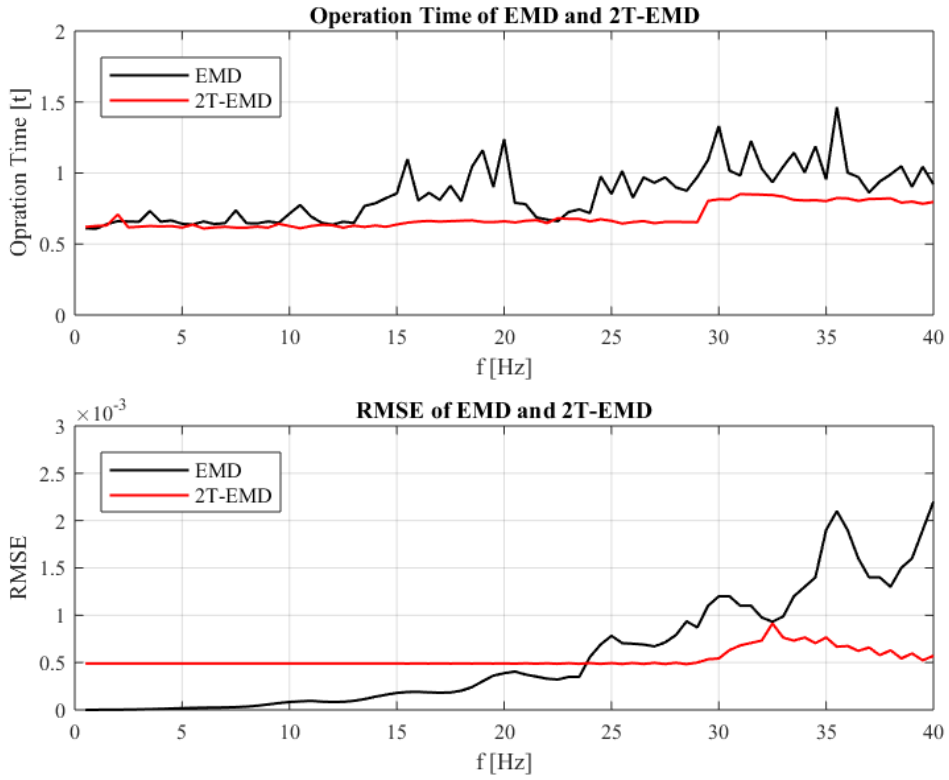

Fig. 2.9 Comparison of operation time and RMSE for EMD and 2T-EMD based on single channel standard artificial signals.

As is shown in the upper panel of figure 2.9, the computational time of 2T-EMD is less than 1s and remains the stable duration range of $0.6\text{s} \sim 0.85\text{s}$, while the computational time of EMD fluctuates greatly in the range of $0.6\text{s} \sim 1.6\text{s}$, and is longer than that of 2T-EMD, even reach twice of 2T-EMD. It takes different computation time to decompose signals of different frequencies for EMD algorithm, while it almost takes the same computation time for 2T-EMD. And as is shown in the lower panel of figure 2.9, the RMSE of EMD is increasing in the range of $4.45 \times 10^{-4} \sim 4.69 \times 10^{-2}$ with the increasing of frequency, while the RMSE of 2T-EMD basically remained stable in the range of $2.20 \times 10^{-2} \sim 3.02 \times 10^{-2}$. So 2T-EMD

has better integrated performance in both computational time and the signal representation accuracy based on single channel standard artificial signals.

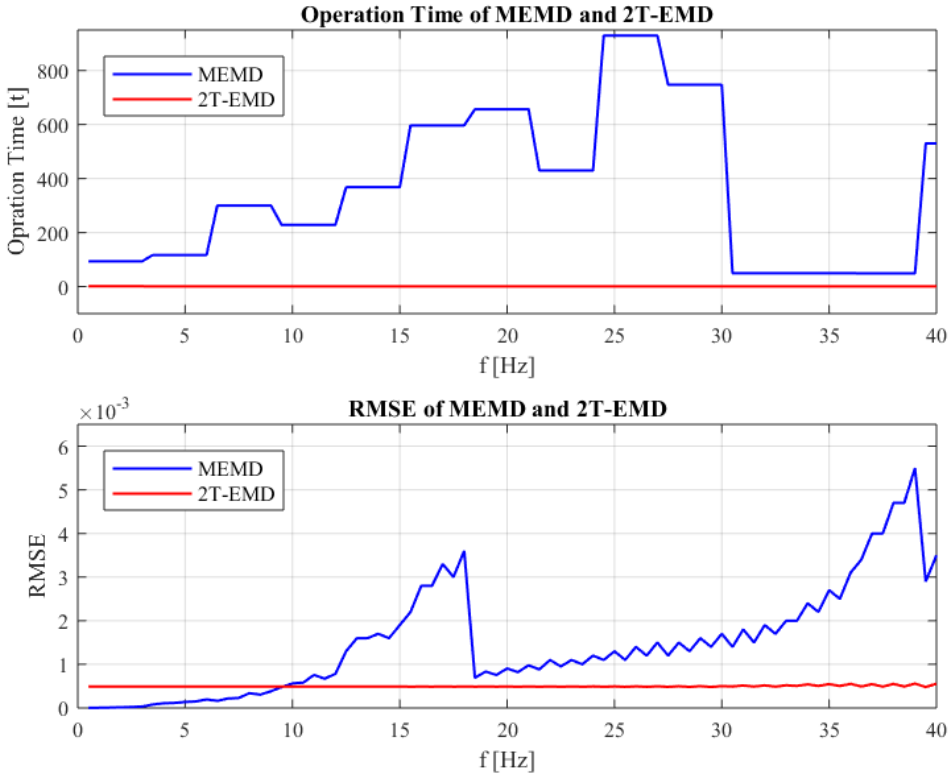

Fig. 2.10 Comparison of operation time and RMSE for MEMD and 2T-EMD based on multi-channels standard artificial signals.

Secondly, computational time and RMSE of MEMD and 2T-EMD based on multi-channel standard artificial signals were compared. In this comparison, the number of multi-channel was set to 6, and the 80 synthetic artificial standard signals mentioned in section 2.1.1 were divided into 13 groups, with 6 channels per group from low to high frequency.

B. Results Based on Coma and Brain-Death Patients' EEG

In the second part, the computational time of EMD, MEMD and 2T-EMD based on patients' EEG explained in section 2.1.2 were compared. And it was also divided into two aspects, where one is comparison between EMD and 2T-EMD based on patients' EEG of single channel, the other is comparison between MEMD and 2T-EMD based

on patients' EEG of multi-channel.

Firstly, EMD and 2T-EMD are used to analyze 36 cases of patients' EEG data for random single channel. As is shown in figure 2.11, the computational time of 2T-EMD algorithm is 1.5s ~2.0s, slightly shorter than that of EMD algorithm, which is in the range of 1.9s ~6.8s. So it takes shorter time to process single channel EEG for 2T-EMD compared with EMD.

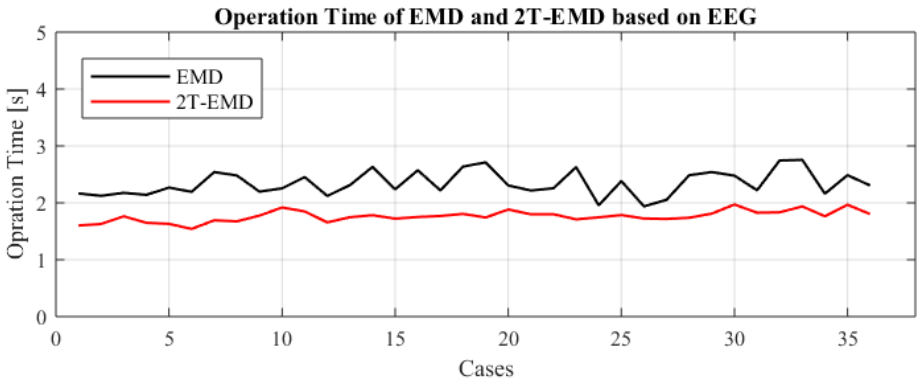

Fig. 2.11 Comparison of operation time for EMD and 2T-EMD based on 36 cases of coma and brain-death patients' EEG.

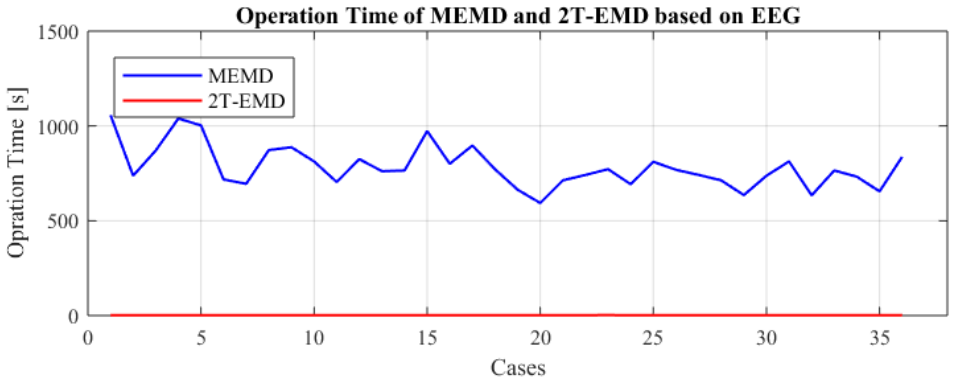

Fig. 2.12 Comparison of operation time for MEMD and 2T-EMD based on 36 cases of coma and brain-death patients' EEG.

Secondly, MEMD and 2T-EMD were used to decompose the 36 cases of coma and brain-death patients' EEG data for 6 channels. As is shown in figure 2.12, the operation time of 2T-EMD is only in the range of 1.6s ~ 2.2s, while that of MEMD is up to 1120s and the time is in the range of 593s ~ 1120s. It is obvious that the

2T-EMD algorithm works much faster than MEMD algorithm for multi-channel EEG.

In summary, it is obvious that the optimal computational performance of 2T-EMD is the best among EMD, MEMD, 2T-EMD for both single and multi-channel signals [33].

2.3.2 Results of Dynamic 2T-EMD Based on Patients' EEG

In this section, the EEG of 35 coma and brain-death patients (male: 21; female: 14) with a total of 36 cases of EEG (coma: 19; quasi-brain-death: 17) were processed by Dynamic 2T-EMD and descriptive statistics measure, in order to obtain the differences of EEG energy between coma patients and brain-death patients. Specifically, it was explained from overall and individual aspects. Firstly, in order to give an overall dynamic EEG energy distribution results for coma group and brain-death group, 60s EEG data were randomly selected from every of 36 cases of coma and brain-death EEG, and analyzed by Dynamic 2T-EMD and descriptive statistics measure. Secondly, from individual point of view, two typical cases of EEG from two different patients who were in coma and brain-death state respectively, and one special patient whose EEG was from coma state to brain-death state were processed by Dynamic 2T-EMD.

A. Results for 36 Cases of Coma and Brain-Death Patients' EEG

Since coma and brain-death patients' EEG data were recorded in the ICU, which were mixed with complex noise, statistical analysis visual analysis were used to analyze the energy data processed by Dynamic 2T-EMD to improve the accuracy and reliability of results. In this paper, we focused on visual descriptive statistical analysis method. Descriptive statistics are summary statistics that quantitatively describe or summarize features of a collection of information [34]. Here basic measures of descriptive statistics including measure of central tendency and measure of dispersion

were applied to evaluate dynamic energy data obtained, in which mean and median were used to describe the central tendency of data set, and standard deviation and percentile were introduced to evaluate the dispersion of data set.

Descriptive statistical analysis was conducted to EEG energy features processed by Dynamic 2T-EMD. Specifically, since duration of every case of EEG was different, 60s EEG data were selected from 19 cases of EEG in coma state and 17 cases of EEG in brain-death state to process by using Dynamic 2T-EMD algorithm to extract EEG energy features firstly. And EEG energy features obtained were grouped from three aspects, which were different cases, different channels, and different states respectively. And then the EEG energy features grouped were evaluated by applying descriptive statistical analysis.

There were 4 steps to conduct the experiment measure:

(1) Select randomly 60s EEG data from 36 cases of coma and quasi-brain-death patients' EEG (coma: 19; quasi-brain-death: 17). Here there were 5 channels of EEG data with values equal 0 from 3 cases of EEG invalid.

(2) Process these EEG data by applying Dynamic 2T-EMD algorithm and 211 time-energy series (36 cases $\times$ 6 channels - 5 invalid series) were obtained.

(3) Group the 211 time-series according to 3 ways:

① Divide the 211 time-series into 36 groups according to 36 cases.

② Divide the 211 time-series into 12 groups according to 2 states and 6 channels.

③ Divide them into 2 groups according to 2 states.

(4) Analyze time-energy series after grouping by using descriptive statistical analysis, in which the mean and median were computed to evaluate the central tendency and the standard deviation and quantile were computed to evaluate the dispersion of data.

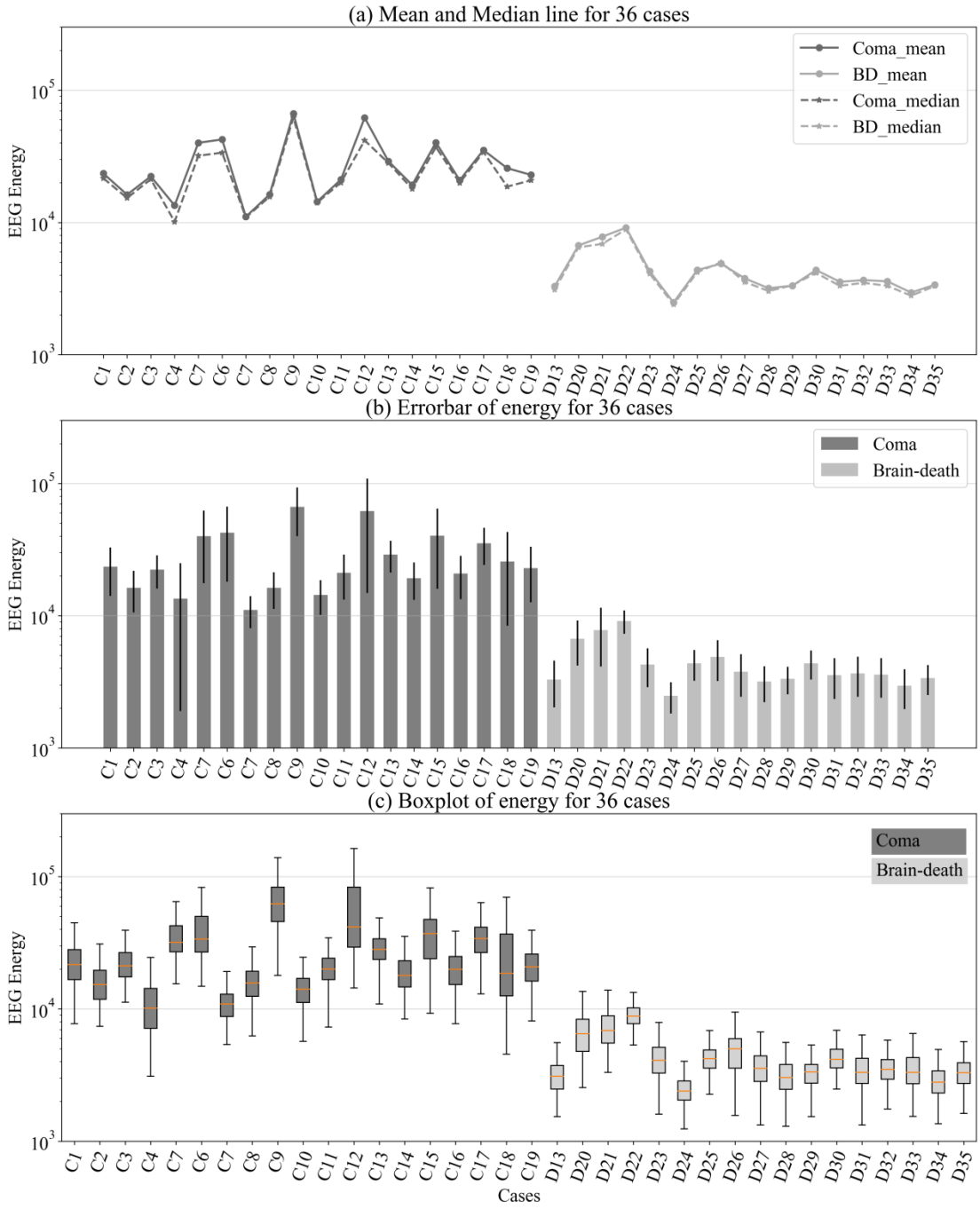

Fig. 2.13 The statistical analysis results of EEG energy for 36 coma and quasi-brain-death EEG for average channel.

a. Static Statistical Results for 36 Cases of Patients' EEG

In this part, 211 time-energy series were grouped into 36 set of data based on cases. The mean, median, standard deviation and quantile were computed for every case for average channel. As shown in figure 2.13(a), it is intuitively observed that the mean

and median of EEG energy for coma case is higher than that for brain-death case for average channel. Here the mean and median energy fluctuation range of coma cases are $1.10 \times 10^4 \sim 6.66 \times 10^4$ and $1.01 \times 10^4 \sim 6.22 \times 10^4$, which are higher than 1.00×10^4, while the mean and median energy fluctuation range of brain-death cases are $2.48 \times 10^3 \sim 9.13 \times 10^3$ and $2.40 \times 10^3 \sim 8.86 \times 10^3$, which are no lower than 1.00×10^4. Moreover, it is also shown that the variance range of standard deviation of coma cases is wider than that for brain-death cases from figure 2.13(b) and figure 2.13(c).

b. Static Statistical Results Based on 2 States – 6 Channels

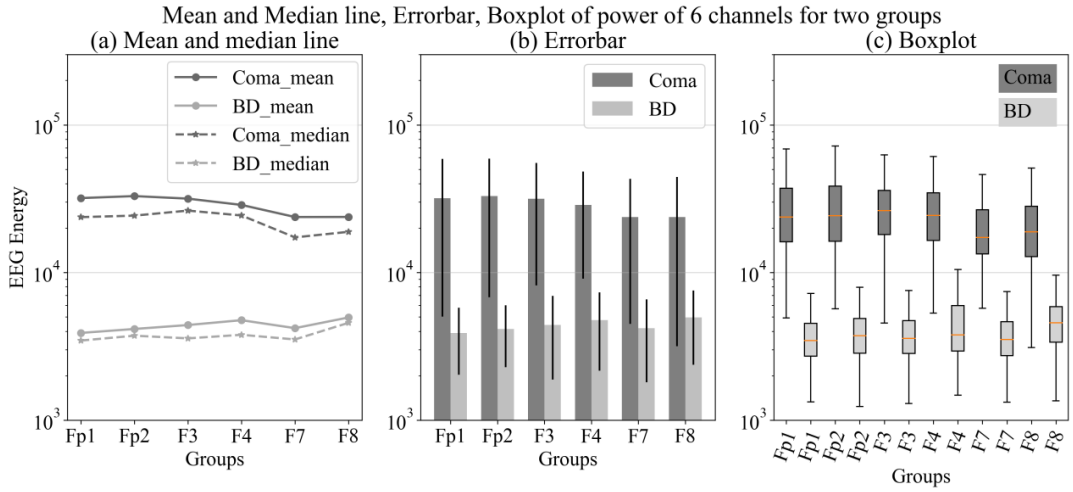

Fig. 2.14 The statistical analysis results of EEG energy for coma group and quasi-brain-death group at each channel.

In order to get characteristics of EEG energy for coma group and brain-death group in different channels of this batch of EEG energy data, 211 time-energy series were grouped into 12 set of data based on 2 states and 6 channels. Mean, median, standard deviation and quantile were also calculated for the 12 set of data. As shown in figure 2.14(a), (b) and (c), it is obviously observed that the mean and median of coma group is higher than that of brain-death group for every channel, and the range of energy change of every channel for coma group is wider than that for brain-death group. Moreover, values of mean, median and fluctuation percent between mean and median

value of every channel for 2 groups were shown in Table 2-2 and table 2-3, in which percent is defined as $percent = \frac{(Mean-Median)}{Mean}$, it is used to measure the difference between mean and median value. In general, it is shown that the percent for brain-death group is lower compared with the percent for coma group.

Table 2-2 Mean, median and percent of EEG energy for coma group at every channel.

Coma	Channel					
	Fp1	**Fp2**	**F3**	**F4**	**F7**	**F8**
Mean	31946	32951	31666	28708	23772	23804
Median	23735	24299	26274	24351	17303	18872
Percent	25.7%	26.3%	17.0%	15.18%	27.2%	20.7%

Table 2-3 Mean, median and percent of EEG energy for brain-death group at every channel

Brain-death	Channel					
	Fp1	**Fp2**	**F3**	**F4**	**F7**	**F8**
Mean	3899	4147	4410	4756	4201	4962
Median	3461	3734	3581	3787	3521	4564
Percent	11.23%	9.96%	18.80%	20.37%	16.19%	8.02%

Here the characteristics of energy for coma group and brain-death group for average channel were shown in figure 2.15, in which there were 114 time–energy series (19 cases × 6 channels - 5 invalid series) for coma group and 102 time-energy series (17 cases × 6 channels) for brain-death group. As can be seen from figure 2.15 (a) and figure 2.15 (b), the distribution of energy data for coma group is intuitively higher than that for brain-death group, in which the mean of both group are 2.88×10^4 and 4.40×10^3, and the median of both group are 2.24×10^4 and 3.73×10^3 respectively. Furthermore, the distribution of energy for coma group is obviously dispersed than that for brain-death group.

c. Static Statistical Results Based on 2 States – Average Channel

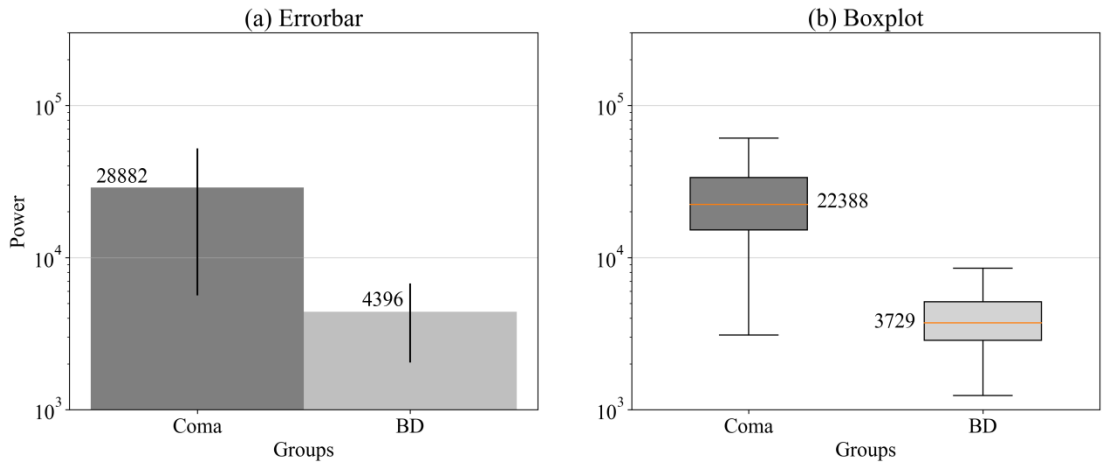

Fig. 2.15 The error bar and box plot of coma group and brain-death group for average channel.

d. Dynamic Statistical Results Based on 2 States – Average Channel

In this part, 19 cases of EEG data for coma group and 17 cases of EEG data for brain-death group were analyzed by Dynamic 2T-EMD. Here the time window of Dynamic 2T-EMD was set to 1s and no overlap among time windows. Then we took mean value, 5 quantile values (5%, 25%, 50%, 75%, and 95%) of every second for channels averaged for coma group and brain-death group respectively due to the two groups were not balanced. As shown in figure 2.16, it is obviously observed that the dynamic EEG energy distribution of channels averaged for coma group is higher than that for brain-death group.

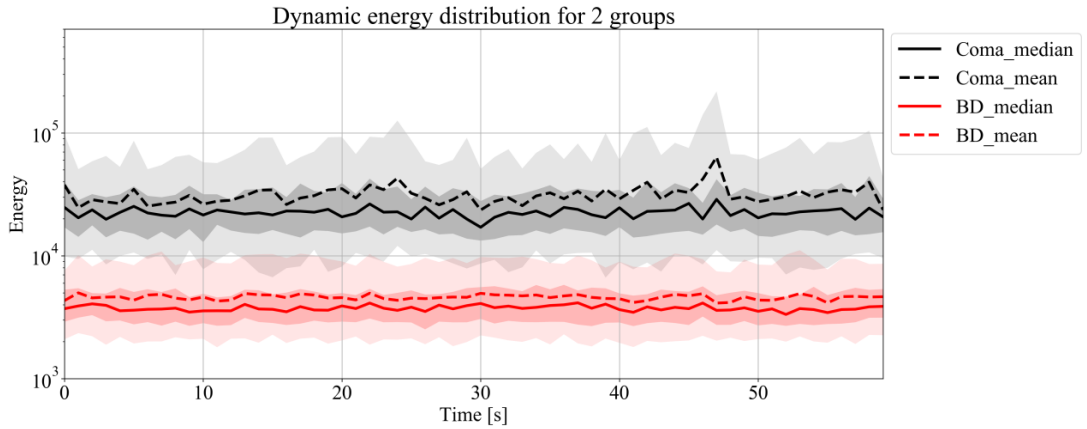

Fig. 2.16 Dynamic EEG energy distribution of coma group and brain-death group for

averaged channels. Coma group is marked in black and brain-death group is marked in red. Thick lines show median line of data. Thick dashed lines show mean line of data. Dark filled bands highlight 25%-75% of data. Light filled bands highlight 5%-95% of data.

And as shown in figure 2.17, we also analyzed the dynamic EEG energy distribution for every channel (Fp1, Fp2, F3, F4, F7 and F8) for both coma group and brain-death group. It is shown there exists significant differences of EEG energy distribution among different channels for coma group and brain-death group.

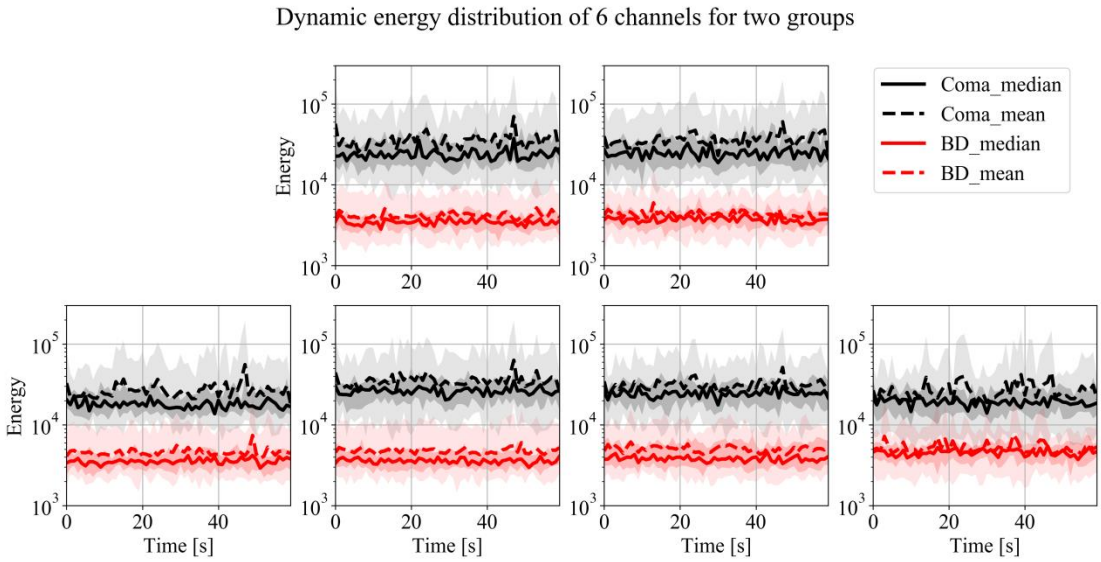

Fig. 2.17 Dynamic EEG energy distribution of coma group and brain-death group for 6 channels.

A. Results for 2 Typical Cases and 1 Special Case of Patients' EEG

a. Results for 2 Typical Cases of Coma and Brain-Death Patients' EEG

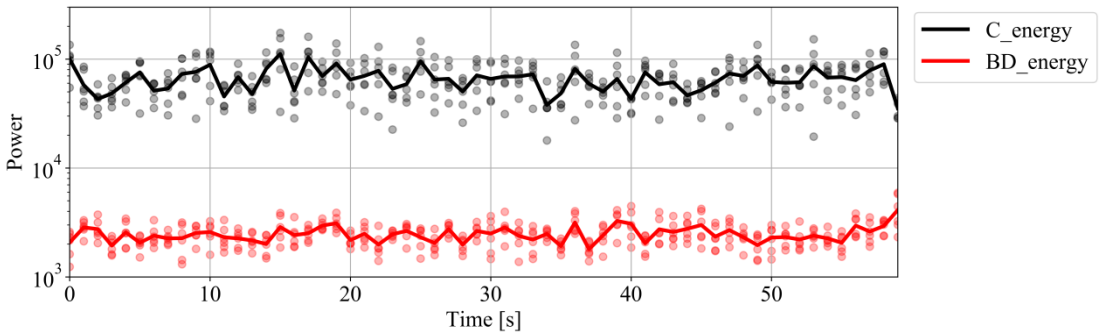

Fig. 2.18 Dynamic EEG energy distribution of average channel for one coma patient.

In this part, we selected 60s EEG data from the coma patient's EEG with recording time of 937s as well as 60s EEG data from the brain-death patient's EEG with recording duration of 905s. As is shown in figure 2.18, it is intuitively observed the dynamic change of EEG energy for the two typical cases. The range of dynamic EEG energy of the coma patient's EEG is $3.5 \times 10^4 \sim 1.1 \times 10^5$, while it's $1.8 \times 10^3 \sim 4.1 \times 10^3$ for the brain-death patient's EEG.

a. Results for 1 Special Cases of Patient's EEG from Coma State to Brain-Death State

Moreover, the special patient's EEG whose state was from coma to brain-death state was processed, in which 60s EEG data from coma EEG segment and 60s EEG data from brain-death segment were selected to analyzed by Dynamic 2T-EMD. As is shown in figure 2.18, for the same patient, the EEG energy distribution for coma state is higher than that for brain-death state, which is consistent with that for coma group and brain-death group. And the distribution range of EEG energy for the special patient' EEG decreases from $1.7 \times 10^4 \sim 4.1 \times 10^4$ to $2.4 \times 10^3 \sim 5.8 \times 10^3$ [35].

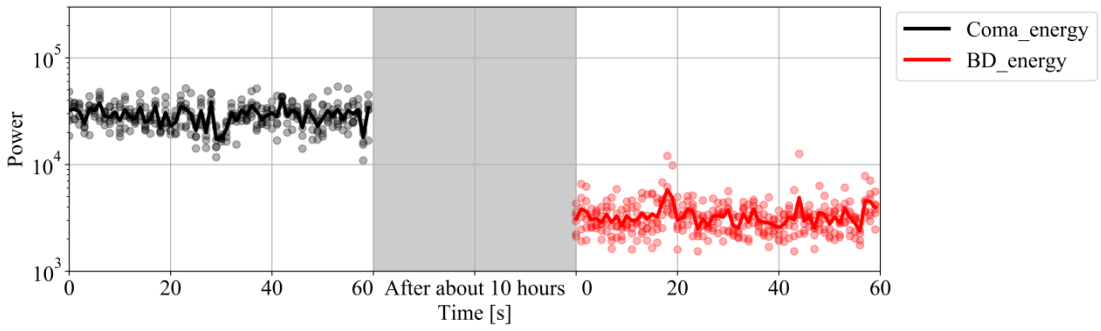

Fig. 2.18 Dynamic EEG energy distribution of average channel for the patient who was from coma state to brain-death state.

2.4 Chapter Summary

In this chapter, three static EMD-based EEG energy extracted algorithms (EMD, MEMD, 2T-EMD) were compared to illustrate the advantage of 2T-EMD algorithm

from algorithm principle and experiments, where experiments based on both standard artificial signals and quasi-brain-death patients' EEG respectively. Hereafter, the Dynamic 2T-EMD algorithm is firstly proposed by dynamically extending 2T-EMD. Then 36 cases of coma and brain-death patients' EEG were analyzed by the proposed algorithm. Moreover, two typical patients' EEG who were in coma state and in brain-death state respectively, as well as one special patient's EEG who was from coma state to brain-death state were also analyzed by Dynamic 2T-EMD from individual perspective. EEG energy features obtained then analyzed by descriptive statistical measure. Final results illustrated that there was a significant differences of EEG energy between coma patients' EEG and brain-death patients' EEG.

Chapter 3 Epilepsy EEG Analysis

3.1 Materials

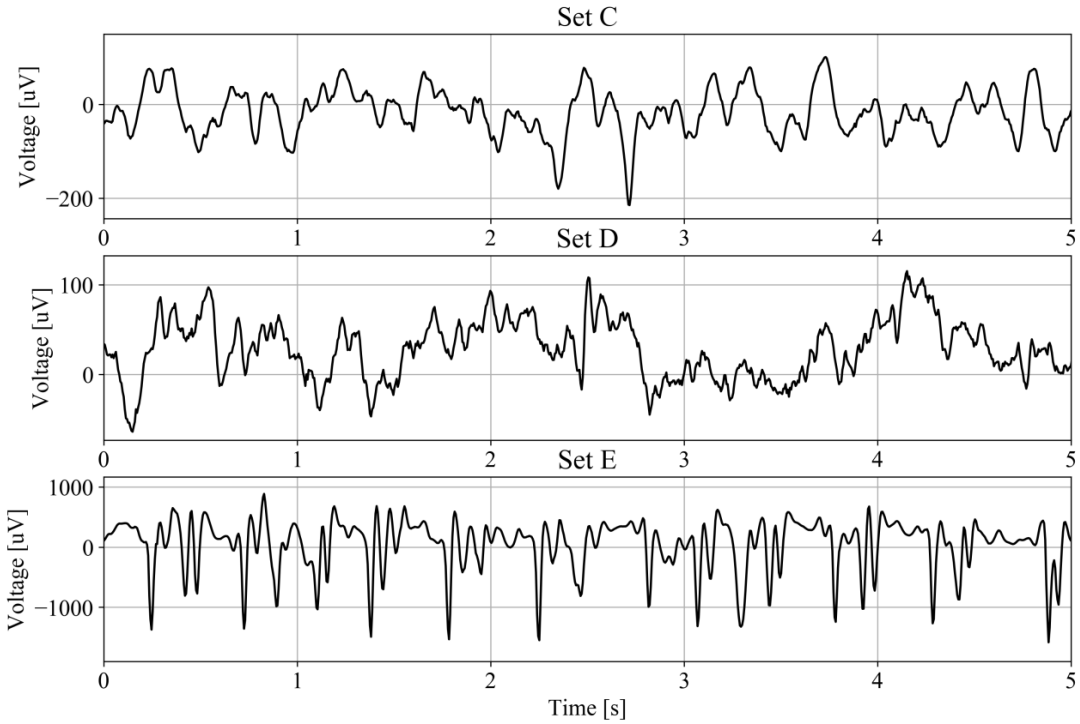

Fig. 3.1 EEG time series of Bonn dataset

The epilepsy EEG dataset used in this paper is from the Department of Epileptology at the University of Bonn [36]. The dataset is public available and used widely in the research of epilepsy EEG data analysis and classification. There were 5 sets in the dataset, denoted as set A, set B, set C, set D and set E. Each of set contained 100 single-channel EEG segments with recording duration of 23.6s per segment. The sampling rate and band-pass filter were set 173.61Hz and 0.53~40Hz. In details, set A and set B were surface EEG recordings taken from five healthy volunteers who were relaxed in an awake state with eyes open (A set) and eyes closed (B set). Set C, set D and set E were intracranial EEG recordings originated from five patients, in which set C and set D were taken from during seizure free intervals from the opposite of the hemisphere of the brain (set C) and within epileptogenic zone (set

D), set E were taken from epileptic seizure activity. In this part, C set, D set and E set were studied. As shown in figure 3.1 is the EEG time series of C set, D set and E set for Bonn dataset.

3.2 Methodology

3.2.1 Phase-Amplitude Coupling

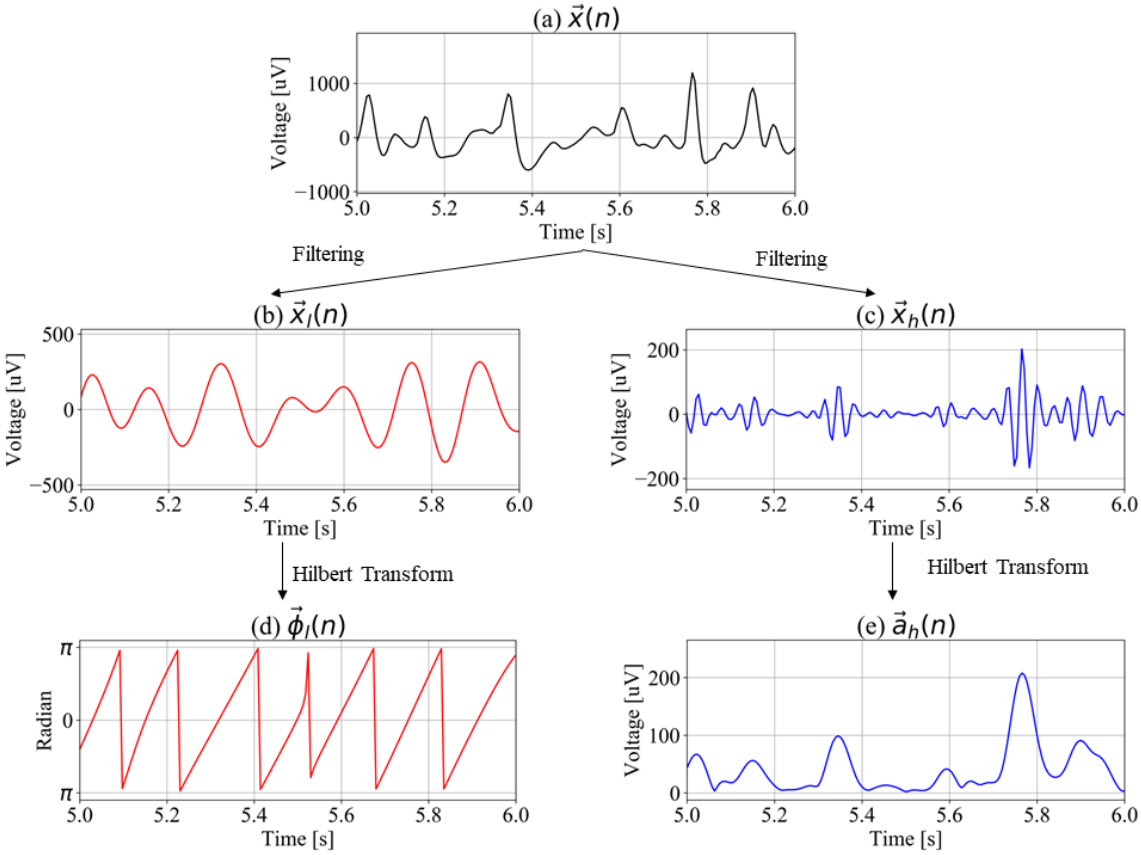

Fig. 3.2 The process of filtering and Hilbert Transform. (a) was the single-channel time series $\vec{x}(n)$ $(n = 1, \dots, N)$. (b) and (c) were the low-frequency oscillation $\overrightarrow{x_l}(n)$ and high-frequency oscillation $\overrightarrow{x_h}(n)$ filtered by band-pass filter, where the range of low-frequency and high-frequency were set to 4Hz – 8Hz and 30Hz – 40Hz. (d) and (e) were low-frequency phase time series $\overrightarrow{\emptyset_l}(n)$ and high-frequency amplitude time series $\overrightarrow{a_h}(n)$ computed by Hilbert Transform.

Phase-amplitude coupling is explained as that the high-frequency amplitude is modulated by the low-frequency phase. Low-frequency phase time series and

high-frequency amplitude time series were computed firstly before evaluating the phase-amplitude coupling strength. In this paper, band-pass filtering and Hilbert Transform were used, in which FIR (finite impulse response) filters was applied to filter. Take an example, for a single-channel time series $\vec{x}(n)\ (n = 1, \dots, N)$, band-pass filtered was applied to extracted high-frequency oscillation interested $\overrightarrow{x_h}(n)$ and low-frequency oscillation interested $\overrightarrow{x_l}(n)$. Then Hilbert Transform was used to extract corresponding instantaneous phase and instantaneous amplitude of both oscillations. As shown in formula (3-1), we got two analytic signals.

$$\begin{aligned} \overrightarrow{z_l}(n) &= \overrightarrow{a_l}(n)e^{i\overrightarrow{\emptyset_l}(n)}, \qquad \overrightarrow{a_l}(n) = |\overrightarrow{z_l}(n)| \\ \overrightarrow{z_h}(n) &= \overrightarrow{a_h}(n)e^{i\overrightarrow{\emptyset_h}(n)}, \qquad \overrightarrow{a_h}(n) = |\overrightarrow{z_h}(n)| \end{aligned} \tag{3-1}$$

Where $\overrightarrow{\emptyset_l}(n)$ and $\overrightarrow{\emptyset_h}(n)$ were the instantaneous phase time series, as well as $\overrightarrow{a_l}(n)$ and $\overrightarrow{a_h}(n)$ were the instantaneous amplitude time series of both high-frequency oscillation and low-frequency oscillation. It is shown in figure 3.2 that the process of band-pass filtering and Hilbert Transform before computing coupling strength.

A. Modulation Index (MI) of Phase-Amplitude Coupling

There are five methods to quantify the phase-amplitude coupling strength also called MI. The first method was proposed by Canolty et.al, which evaluated phase-amplitude coupling strength by computing the normalized MI [37]. The algorithm is illustrated as Algorithm (3).

Algorithm 3 Phase-amplitude coupling algorithm proposed by Canolty

---

1. Defined a complex variable, where a_h is the amplitude time series of high frequency oscillation, $\overrightarrow{\emptyset_l}$ is the phase time series of low frequency oscillation:

$$\vec{z}(n) = \overrightarrow{a_h}e^{i\overrightarrow{\emptyset_l}(n)}\ (n = 1, \dots, N)$$

---

2. Compute the absolute value of the mean vector based on $\vec{z}(n)$ and defined the result as 'MI':

$$M_{raw} = \left| \frac{1}{N} \sum_{n=1}^{N} \vec{Z}(n) \right|$$

3. Using surrogate data approach to compute the surrogate $\overrightarrow{z_s}(n)$ $(n = 1, \dots, N;\ s = 1, \dots, S)$ by introducing an arbitrary time lag between $\overrightarrow{\emptyset_l}$ and $\overrightarrow{a_h}$. And compute the mean vector $M_s = \left| \frac{1}{N} \sum_{n=1}^{N} \overrightarrow{z_s}(n) \right|$ of $\overrightarrow{z_s}(n)$ as step 2.

4. Repeat the step 3 for $s = 1, \dots, S$ times to obtain the surrogate values $M_1, \dots, M_S$, and compute the mean μ and standard variance σ of these surrogate values.

5. Compute the normalized modulation index which is denoted as M:

$$M = \frac{M_{raw} - \mu}{\sigma}$$

The second method to quantify the phase-amplitude coupling is the PLV (phase-locking value) method [38-40]. The algorithm is illustrated as Algorithm (4).

Algorithm 4 The Phase-amplitude coupling algorithm based on PLV

1. Apply secondly Hilbert Transform to $\overrightarrow{a_h}$, and get the analytic signal of $\overrightarrow{a_h}$ as below:

$$\overrightarrow{Z_{a_h}} = \overrightarrow{a_{a_h}}(n) e^{i\overrightarrow{\emptyset_{a_h}}(n)} \ (n = 1, \dots, N)$$

Where $\overrightarrow{a_{a_h}}(n)$ and $\overrightarrow{\emptyset_{a_h}}(n)$ are the amplitude time series and phase time series of $\overrightarrow{a_h}(n)$.

2. The PLV is defined as:

$$PLV = \left| \frac{1}{N} \sum_{n=1}^{N} e^{i(\overrightarrow{\emptyset_l}(n) - \overrightarrow{\emptyset_{a_h}}(n))} \right|$$

Where the PLV value is used to measure the coupling strength.

The third method to measure the phase-amplitude coupling was based on GLM (general linear model) [41]. The algorithm is explained in Algorithm (5).

Algorithm 5 The Phase-amplitude coupling algorithm based on GLM

1. Create a new high-frequency amplitude model by introducing a multiple regression as below and compute the residual vector $\vec{e}$.

$$\overrightarrow{a_h} = \vec{X}\vec{\beta} + \vec{e}$$

Where $\vec{X} = \begin{bmatrix} cos(\overrightarrow{\emptyset_l}(n)) & sin(\overrightarrow{\emptyset_l}(n)) & 1 \\ & & \vdots \\ & & 1 \end{bmatrix}_{N \times 3}$ $(n = 1, \dots N)$, $\overrightarrow{\beta}$ are regression coefficients by using Least-Squares solution, $cos(\overrightarrow{\emptyset_l}(n))$ and $sin(\overrightarrow{\emptyset_l}(n))$ are the cosine and sine transform of low-frequency phase time series respectively.

2. Compute the value described as the model:

$$r_{GLM}^2 = \frac{SS(\overrightarrow{a_h}) - SS(\vec{e})}{SS(\overrightarrow{a_h})}$$

Where $SS(A_h)$ and $SS(e)$ are the sum of squares of high-frequency amplitude time series $\overrightarrow{a_h}$ and the sum of squares of error $\vec{e}$. The r_{GLM}^2 is used to quantify the coupling strength.

The fourth method to measure the phase-amplitude coupling was based on an adaptive of the KL distance (Kullback-Leibler distance) [42]. The algorithm is explained in Algorithm (6).

Algorithm 6 The PAC algorithm based on an adaptive of the KL distance

1. Construct the composite time series $[\overrightarrow{\emptyset_l}(t) \quad \overrightarrow{a_h}(t)]$, which present the amplitude of low-frequency oscillation at each corresponding phase of the low-frequency rhythm.

2. Divide the phases $\overrightarrow{\emptyset_l}(t)$ into bins in order, and compute the mean value of $\overrightarrow{a_h}(t)$ in each phase bin j, where the mean value is expressed by $\langle a_h \rangle_{\emptyset_l}(j)$.

3. Normalize the mean value $\langle a_h \rangle_{\emptyset_l}(j)$:

$$P(j) = \frac{\langle a_{f_A} \rangle_{\emptyset_{f_P}}(j)}{\sum_{j=1}^{N\_bins} \langle a_{f_A} \rangle_{\emptyset_{f_P}}(j)}$$

Where N_bins is the number of phase bins.

4. There is no coupling between high-frequency amplitude and low-frequency phase if the mean value $\langle a_h \rangle_{\emptyset_l}(j)$ at each phase bin is the same, namely the phase-amplitude distribution P is consistent with uniform distribution U; if different, there is coupling. So a new MI is defined to measure the difference of phase-amplitude distribution and uniform distribution by adapting KL distance. The new MI is described as:

$$MI = \frac{D_{KL}(P, U)}{log(N\_bins)}$$

Where $D_{KL}(P, U) = log(N\_bins) - H(P), \quad H(P) = -\sum_{j=1}^{N\_bins} P(j) log[P(j)]$.

The fifth method to quantify the phase-amplitude coupling strength was proposed by Ozkurt. et.al. [43]. The value to quantify the phase-amplitude coupling strength ρ is defined as below:

$$\rho = \frac{1}{\sqrt{N}} \frac{\left|\sum_{n=1}^{N} a_h(n) e^{i\emptyset_l(n)}\right|}{\sqrt{\sum_{n=1}^{N} a_h(n)^2}} \quad (n = 1, \dots, N) \tag{3-2}$$

B. Phase-Amplitude Comodulogram

Phase amplitude comodulogram is the graphical representation that exhibits coupling strength among multiple bands. It is obtained a series of coupling strengths

over a grid of frequencies. When there is no priori assumption of frequency bands phase-modulating and the amplitude-modulated, the comodulogram can be used to locate initially the frequency bands which coupling occurs. As shown in figure 3.3, the frequency of phase f_P is represented in the horizontal axis and the frequency of amplitude f_A is displayed in the ordinate axis. The phase-coupling strength at the band $[f_A(i) \quad f_P(j)]$ is denoted using a pseudocolor plot with hot color indicating high coupling strength.

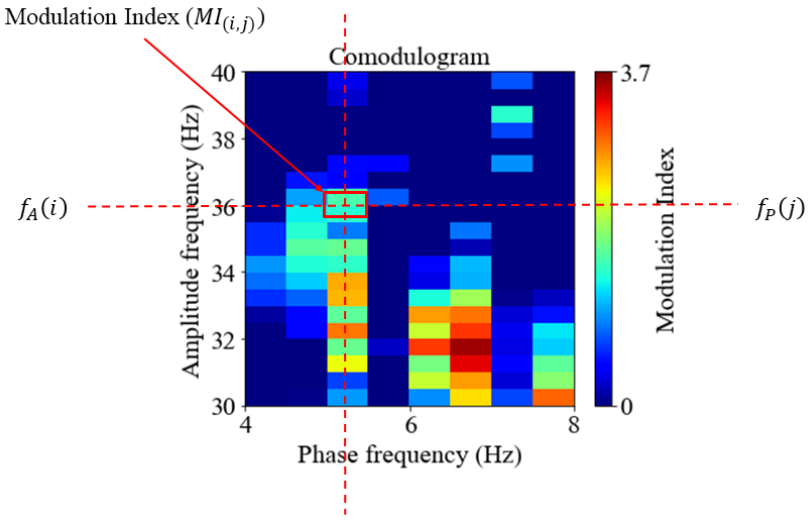

Fig. 3.3 The example of comodulogram.

3.2.2 Support Vector Machine (SVM)

SVM is a supervised learning method based on statistical learning theory (SLT) in machine learning. The basic model is the linear classifier that defines the largest interval in the feature space. It maps the vector to the high-dimensional feature space through nonlinear mapping, and then selects the most classified surface to obtain a hyperplane segmentation, which can separate the two types of modes and ensure the interval is maximized. It is suitable for solving classification problems with low sample size in high-dimensional complex nonlinear systems. For example, as shown in figure 3.4, for a linear classification in two dimensional plane, there is a binary classification as below:

$$\{(x_1, y_1), \cdots, (x_n, y_n)\} \qquad x_n \in R^m, y_i \in \{1, -1\}, i = 1, \cdots, n \tag{3-3}$$

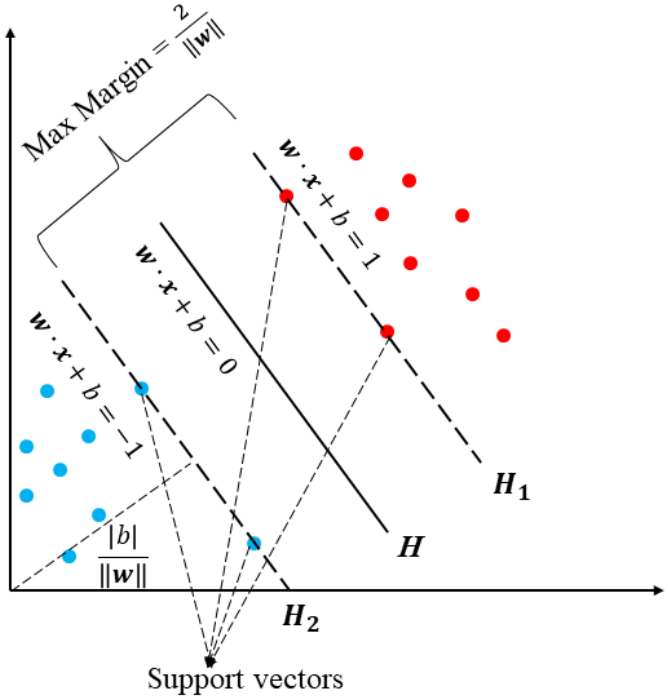

Fig. 3.4 An example of binary classification by using SVM.

Define a hyperplane segmentation $\boldsymbol{H}$ which can divides the samples correctly, as shown in formula (3-4):

$$\boldsymbol{\omega}^T \boldsymbol{x} + b = 0 \tag{3-4}$$

Then selected two others hyperplanes $\boldsymbol{H_1}$ and $\boldsymbol{H_2}$ parallel to $\boldsymbol{H}$ which also can separate the samples. More specifically, the positive samples and negative samples closest to $\boldsymbol{H}$ fall on $\boldsymbol{H_1}$ and $\boldsymbol{H_2}$ respectively, where such the sample is the support vector. Then all other training samples are outside of $\boldsymbol{H_1}$ and $\boldsymbol{H_2}$ respectively. $\boldsymbol{H_1}$ and $\boldsymbol{H_2}$ are defined as formula (3-5) and formula (3-6).

$$\boldsymbol{\omega}^T \boldsymbol{x} + b = 1 \tag{3-5}$$

$$\boldsymbol{\omega}^T \boldsymbol{x} + b = -1 \tag{3-6}$$

And $\boldsymbol{H_1}$ and $\boldsymbol{H_2}$ are met the constraints as formula (3-7) and formula (3-8):

$$\boldsymbol{\omega}^T \boldsymbol{x_i} + b \geq 1 \quad for \quad y_i = 1 \tag{3-7}$$

$$\boldsymbol{\omega}^T \boldsymbol{x_i} + b \leq -1 \quad for \quad y_i = -1 \tag{3-8}$$

Formula (3-7) and formula (3-8) can be unified as below:

$$y_i(\boldsymbol{\omega}^T \boldsymbol{x_i} + b) - 1 \geq 0 \tag{3-9}$$

Then the distance between $\boldsymbol{H_1}$ and $\boldsymbol{H_2}$ can be computed as formula (3-10):

$$Margin = \frac{2}{\|\boldsymbol{w}\|} \tag{3-10}$$

The purpose of the SVM is to find such a hyperplane $\boldsymbol{H}$ to classify the samples into two parts correctly and to maximize the distance between $\boldsymbol{H_1}$ and $\boldsymbol{H_2}$. So the interval Margin is maximized to find the hyperplane $\boldsymbol{H}$, that is to minimize of $\|\boldsymbol{w}\|$, as shown in formula (3-11):

$$Max\ Margin = \frac{2}{\|\boldsymbol{w}\|} \rightarrow min\frac{1}{2}\boldsymbol{w}^T\boldsymbol{w} \tag{3-11}$$

Then the following conditional extreme value problem is constructed:

$$\begin{cases} min\frac{1}{2}\boldsymbol{w}^T\boldsymbol{w} \\ s.t. \quad y_i(\boldsymbol{\omega}^T \boldsymbol{x_i} + b) - 1 \geq 0 \end{cases} \tag{3-12}$$

Lagrange Multipliers is used to solve the problem and construct the Lagrange equation as below, where $\alpha_i \geq 0$.

$$\begin{aligned} L(w, b, \alpha) &= \frac{1}{2}\|\boldsymbol{w}\|^2 - \sum_{i=0}^{l} \alpha_i (y_i(\boldsymbol{w} \cdot \boldsymbol{x_i} + b) - 1) \\ &= \frac{1}{2}\|\boldsymbol{w}\|^2 - \sum_{i=0}^{l} \alpha_i y_i (\boldsymbol{w} \cdot \boldsymbol{x_i} + b) + \sum_{i=0}^{l} \alpha_i \end{aligned} \tag{3-13}$$

And compute the derivation of w and b for L and set the derivation to 0, the following formula are obtained:

$$L\frac{\partial \boldsymbol{L}}{\partial \boldsymbol{w}} = 0 \rightarrow \boldsymbol{w} = \sum_{i=1}^{l} \alpha_i x_i y_i \tag{3-14}$$

$$L\frac{\partial \boldsymbol{L}}{\partial \boldsymbol{b}} = 0 \rightarrow \boldsymbol{w} = \sum_{i=1}^{l} \alpha_i y_i = 0 \tag{3-15}$$

Then substitute formula (3-14) and formula (3-15) into formula (3-13), we can get a new objective function as below, which is the Dural problem of formula (3-13):

$$L_D \equiv \sum_i \alpha_i - \frac{1}{2}\sum_{i,j} \alpha_i \alpha_j y_i y_j x_i \cdot x_j$$

$$\equiv \sum_i \alpha_i - \frac{1}{2}\alpha^T H \qquad where\ H_{i,j} = y_i y_j x_i \cdot x_j$$

$$s.t. \qquad \sum \alpha_i y_i = 0 \quad \& \quad \alpha_i \geq 0 \tag{3-16}$$

3.2.3 *k*-fold ROC Based on Cross-Validations

ROC (receiver operator curve) and AUC (area under curve) were used to evaluate the classification performance of the binary classifier, in order to observe the classification results of phase-amplitude coupling strength at different bands. ROC is the indicator to reflect the relationship between sensitivity and specificity of variables. As shown in figure 3.5, for a binary classifier, the outcomes are labeled either positive (P) or negative (N). While there are four possible outcomes in a binary classifier:

a. TP (true positive): Both the prediction value and the actual value are P;

b. FP (false positive): the prediction value is P but the actual value is N;

c. TN (true negative): the prediction value is N and the actual value is N;

d. FN (false negative): the prediction value is F but the actual value is T.

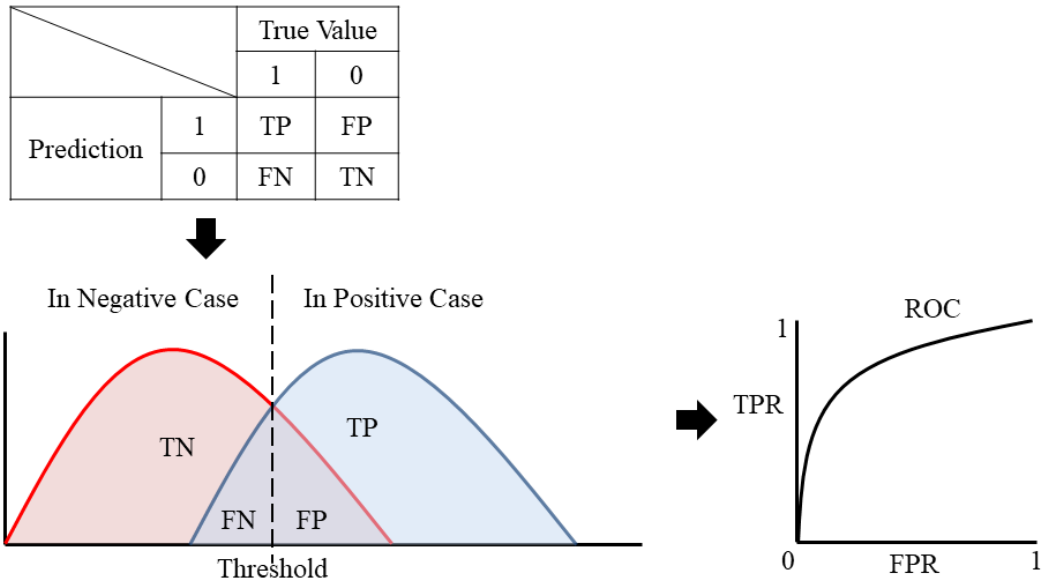

Fig. 3.5 ROC principle diagram.

The sensitivity or TFR (true positive rate) is defined as formula (3-6).

$$TFR = \frac{TP}{TP+FN} \tag{3-6}$$

The specificity or TNR (true negative rate) is defined as formula (3-7).

$$TNR = \frac{TN}{FP+TN} \tag{3-7}$$

So the FPR (false positive rate) is explained as formula (3-8).

$$FPR = 1 - TNR = 1 - \frac{TN}{FP+TN} = \frac{FP}{FP+TN} \tag{3-8}$$

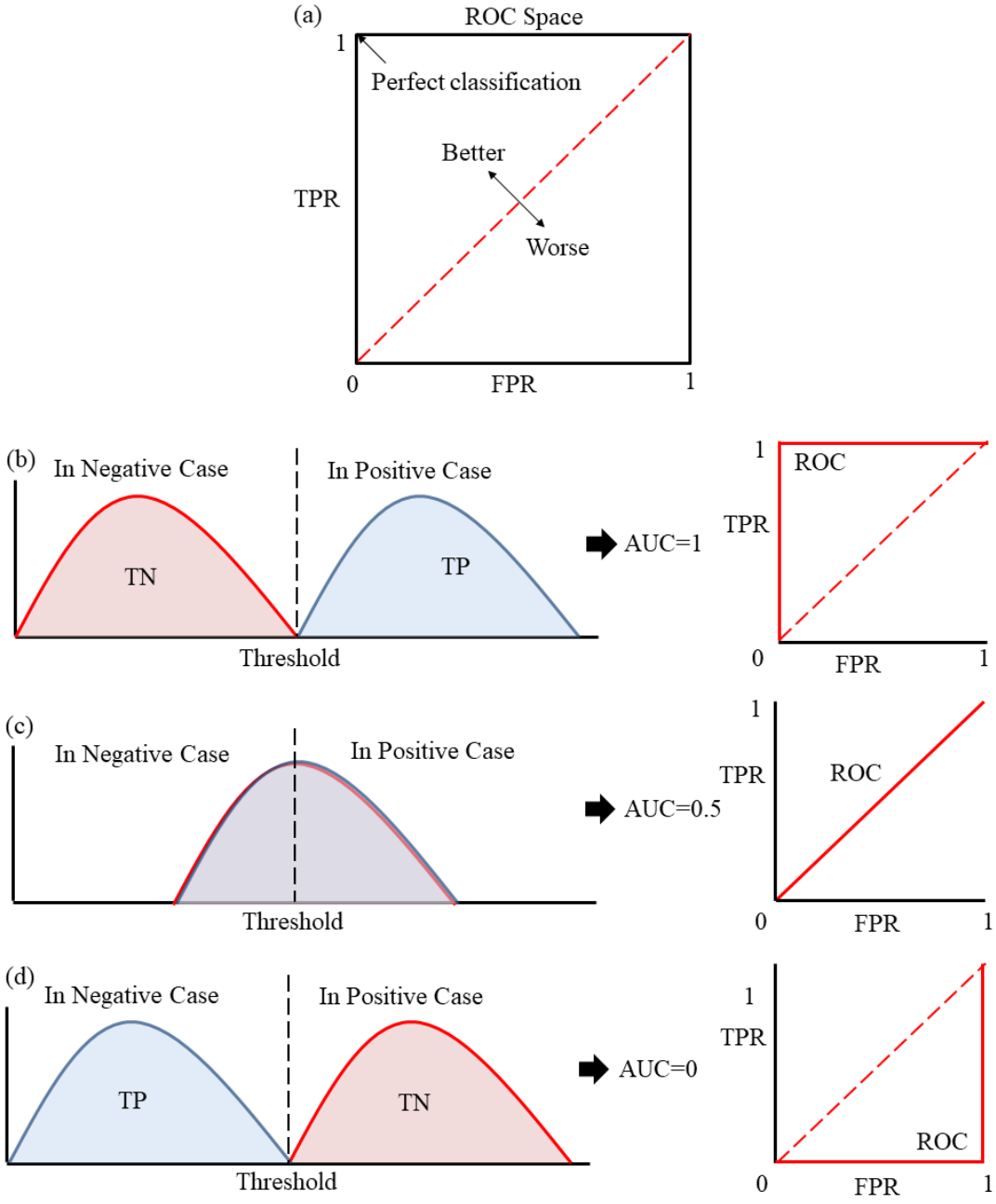

Fig. 3.6 Description of AUC value and three special AUC value.

Cross-validation is a resampling procedure which is used to assess machine learning models on limited data samples. As shown in figure 3.7, for the *k*-fold cross-validation, the dataset is shuffled randomly, and partition the original dataset set into *k* equal subsets, denoted as $f_i(i = 1, \dots, k)$. Then retain the fold f_i as validation set and keep all the remaining *k-1* folds in the cross validation training set. Hereafter train the machine learning model using the cross validation training set and calculate the accuracy of the model by validating the predicted results against the validation set. Repeat the step for *k* times. Finally estimate the accuracy of the model by taking mean of the accuracies derived in all the *k* cases of cross validation.

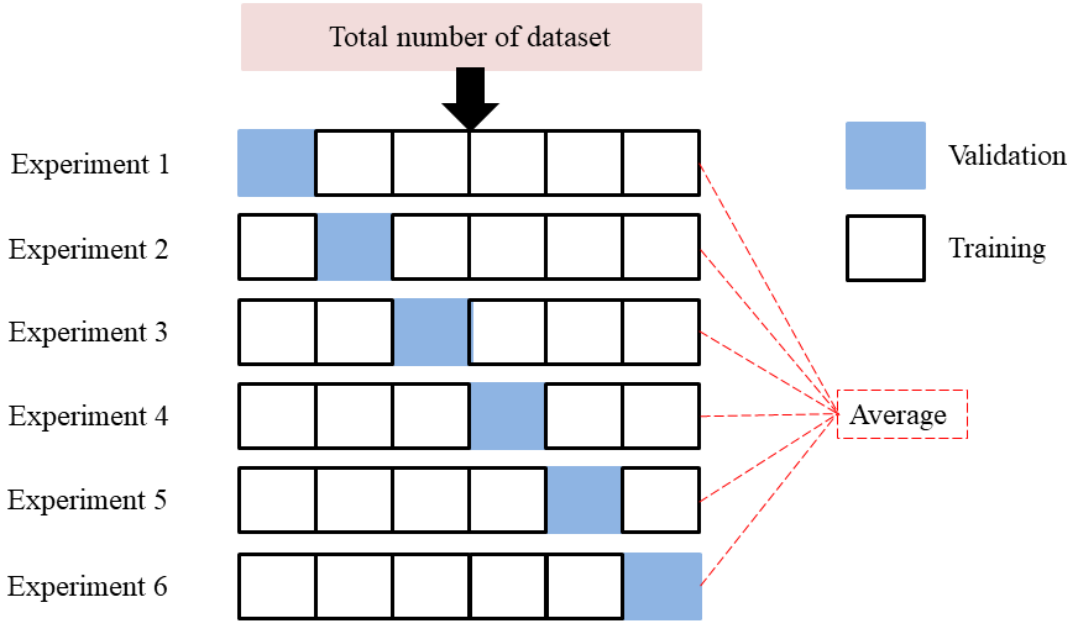

Fig. 3.7 Process of *k*-fold cross-validation.

3.3 Results

3.3.1 Results of Classification Based on MI

In this part, C set, D set and E set of Bonn dataset at 9 bands were be processed by 5 methods of PAC, in which the 5 methods were PAC method of Canolty, PLV, GLM, Tort, Ozkurt, as well as 9 bands were $\delta_l - \alpha$, $\delta_l - \beta$, $\delta_l - \gamma$, $\delta_h - \alpha$, $\delta_h - \beta$, $\delta_h - \gamma$, $\theta - \alpha$, $\theta - \beta$, $\theta - \gamma$. Here $\delta_l - \alpha$ denotes PAC strength between phase of δ_l and

amplitude of α. Then classify the PAC strength by using SVM, where the kernel function is liner. And describe the classification performance by introducing ROC based on k-fold cross-validation, in which $k = 10$. The flow chart of process is as shown in figure 3.8.

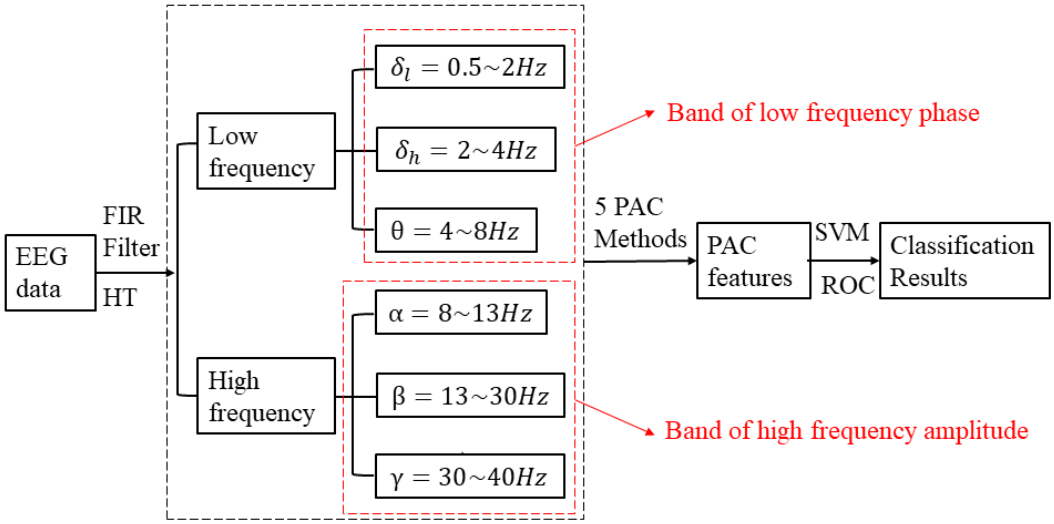

Fig. 3.8 Flow chart of PAC strength processing. HT denotes Hilbert Transform.

Table 3-1 The AUC of PAC for D set and E set based on 5 PAC methods at 9 bands

Method /Bands	$\delta_l - \alpha$	$\delta_l - \beta$	$\delta_l - \gamma$	$\delta_h - \alpha$	$\delta_h - \beta$	$\delta_h - \gamma$	$\theta - \alpha$	$\theta - \beta$	$\theta - \gamma$
Canolty	0.44	0.59	0.63	0.79	0.85	0.84	0.80	0.89	0.92
PLV	0.41	0.72	0.72	0.76	0.85	0.86	0.91	0.93	0.95
GLM	0.54	0.42	0.63	0.77	0.82	0.81	0.91	0.93	0.96
Tort	0.44	0.66	0.30	0.73	0.80	0.85	0.92	0.93	0.94
Ozkurt	0.46	0.50	0.47	0.70	0.78	0.80	0.93	0.92	0.94

From the Table 3-1 and Table 3-2, it is intuitively observed that the AUC at bands $\theta - \beta$, $\theta - \gamma$ are higher, that is to say, there exits obvious coupling strength of seizure activity at bands $\theta - \beta$, $\theta - \gamma$. Typically, the classify accuracy of detecting seizures is up to 0.96 at band $\theta - \gamma$ within epileptogenic zone by using PLV to evaluate PAC strength. Moreover, the accuracy to detect seizures reaches 0.99 at band $\theta - \gamma$ for C set and E set. Furthermore, the results processed by 5 different methods

of computing PAC were close.

Table 3-2 The AUC of PAC of C set and E set based on 5 PAC methods at 9 bands

Method /Bands	$\delta_l - \alpha$	$\delta_l - \beta$	$\delta_l - \gamma$	$\delta_h - \alpha$	$\delta_h - \beta$	$\delta_h - \gamma$	$\theta - \alpha$	$\theta - \beta$	$\theta - \gamma$
Canolty	0.60	0.72	0.78	0.87	0.92	0.90	0.84	0.97	0.97
PLV	0.60	0.80	0.84	0.85	0.94	0.92	0.92	0.98	0.98
GLM	0.60	0.74	0.73	0.85	0.91	0.89	0.91	0.98	0.98
Tort	0.53	0.81	0.89	0.89	0.96	0.98	0.95	0.99	0.99
Ozkurt	0.56	0.71	0.74	0.82	0.90	0.89	0.95	0.98	0.99

3.3.2 Results of Comodulogram

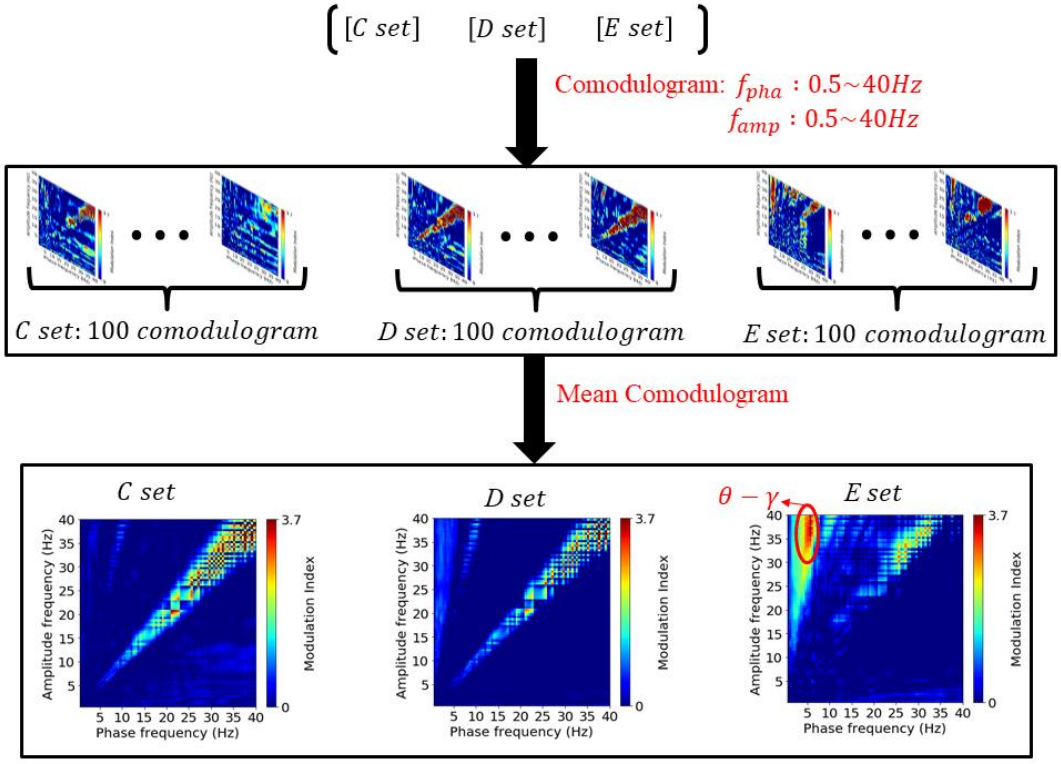

Fig. 3.9 The computation of mean comodulograms for Bonn dataset based on the PAC methos of Canolty .

In this part, we observe intuitively the differences of PAC features of seizure activity and seizure free intervals. So we analyzed C set, D set and E set to search for the features. For each single-channel of each group, The comodulogram is obtained by representing MI values of multiple $[f_A(i) \quad f_P(j)]$ pairs, with both $f_A(i)$ and

$f_P(j)$ being calculated in 0.5 Hz steps with 0.5 Hz bandwidths in frequency range 0.5~40Hz. Then 100 comodulograms for each set were obtained. Finally, in order to search for the differences of PAC for each state, mean values were taken for each set.

As shown in figure 3.9, compared with mean comodulograms of C set and D set, it is significantly shown that there exists strong coupling in $\theta - \gamma$ band for E set, which is consistent with the results illustrate in section 3.3.1.

3.4 Chapter Summary

In this chapter, epilepsy EEG from Bonn dataset were analyzed by 5 phase-amplitude coupling methods at 9 different bands to evaluate the differences of phase-amplitude coupling strength between seizure activity and seizure-free intervals at different bands. The coupling strength features at different bands computed by different PAC methods were extracted and classified by SVM. Classification results were then denoted by *k*-fold ROC based on cross-validation. Final results were shown that the classification accuracy was the highest at $\theta - \gamma$ band, that was to say, there existed stronger phase-amplitude coupling strength in EEG during seizure activity at $\theta - \gamma$ band compared with EEG during seizure-free intervals. Hereafter, the results processed by 5 different methods of computing PAC were similar. Moreover, the results were also visually verified via phase-amplitude comodulogram.

Chapter 4 Realization of Online Diagnostic System

4.1 Introduction

The patients' EEG analysis illustrated in Chapter 2 and Chapter 3 is based on offline EEG data, which is convenient to provide timely doctors analysis results for supporting clinic application. So in this part, an online diagnostic system based on current algorithms is proposed to realize the online monitoring of patients' status. In this system, we develop the online analysis algorithms based on the API of g.USBamp for Matlab to realize online recording and analysis of EEG. And we add a reminder function in the interface to remind the user to take corresponding measures in time when a certain result exceeds the preset threshold. The chapter provides a brief introduction to the composition and implementation of the online diagnostic system.

4.2 Online Diagnostic System Platform

4.2.1 Composition of System

The online diagnostic system comprises two devices, an EEG recording device and a laptop, in which the g.USBamp is used to record EEG. The g.USBamp is a multimodal biosignal amplifier which has 4 potential separated groups with 4 input channels, one reference input and one ground input for each group. And the g.USBamp can connect a PC or notebook via USB (universal serial bus). It also provides a programming API (application programming interface) for Matlab to online record biosignal and develop online analysis algorithms or software.

The software of this system is Malab. Matlab is a programming language developed byMathworks, with powerful computing functions and a large number of stable algorithms toolbox. Therefore, it is used as a tool for physiological data

analysis in the system.

Under the circumstance of operating system of Windows 7, we use Matlab7.9 to develop online EEG analysis algorithms based on the API.

4.2.2 Framework of System

It is shown in figure 4.1, the framework of system consists 3 modules, online EEG recording, online EEG analysis and online results display respectively. In the module of online EEG recording, EEG data is recorded by using g.USBamp device, and transferred online to PC or notebook via USB. Then EEG analysis algorithms in Matlab and EEG data are called and the features of EEG data are extracted and processed by the algorithm in the module of online EEG analysis. Finally the results of the analysis are visually displayed on the interface in the module of online results display. Based on the platform, EEG recording, feature extraction and analysis can be achieved, and finally user-friendly results are obtained.

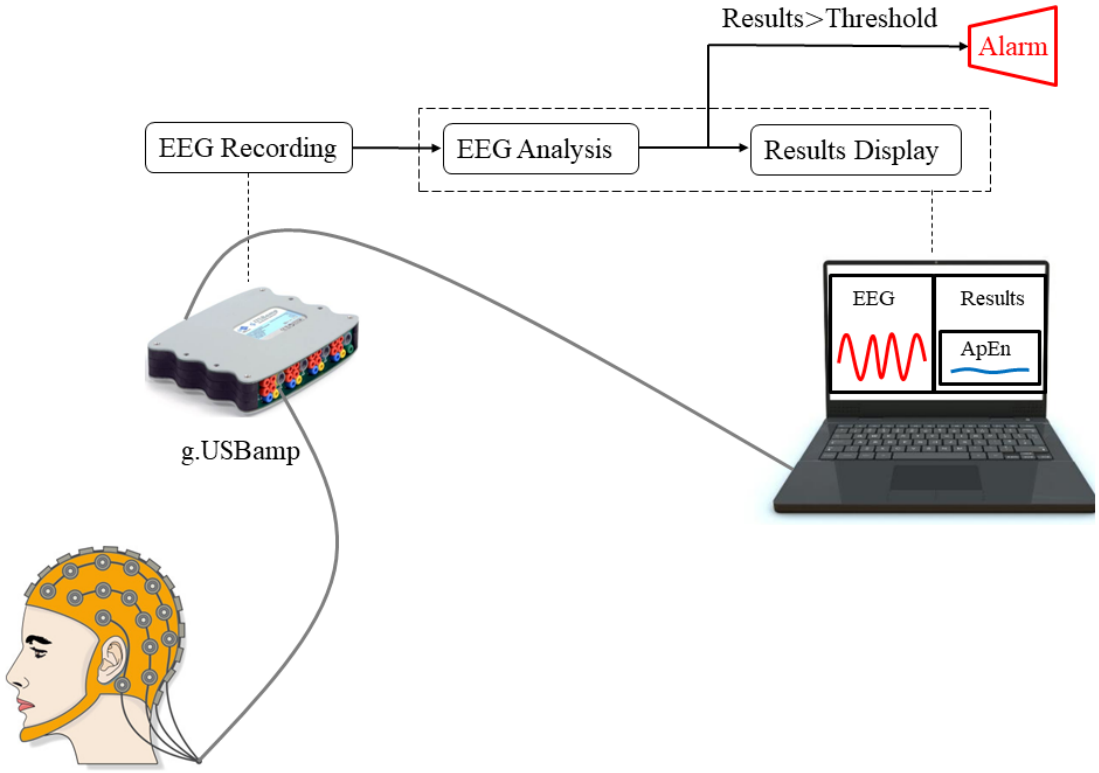

Fig. 4.1 The framework of online EEG diagnostic system.

In the framework of system, the important part is the online EEG analysis algorithm, which mainly consists of calling online recording signals and then calling existed function to analyze the signals. Here the existed algorithms mainly involve algorithms based on EEG energy features extraction such as EMD-based algorithms, as well as algorithms based on complexity features extraction such as ApEn (approximate entropy) and SampEn (sample entropy). The flow chart of online analysis algorithm is shown in figure 4.2. Specifically, there are 4 properties to set in the configure properties:

(1) Set the sampling frequency and the recording time of g.USBamp;

(2) Connect the ground sockets and reference sockets of groups A, B to common ground and reference, since there are 6 electrodes in experiment;

(3) Set the bandpass filter;

(4) Set the notch filter.

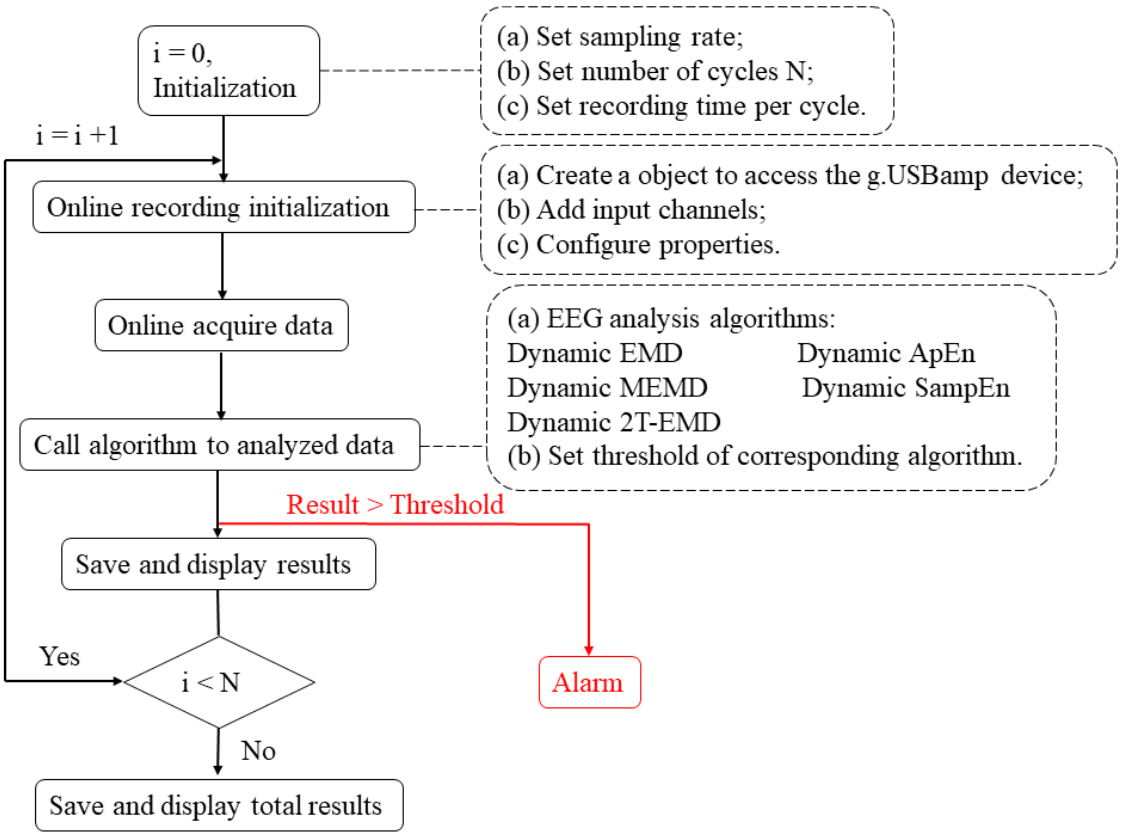

Fig. 4.2 Flow chart of online EEG analysis algorithm.

4.3 Experiment

4.3.1 Experiment Setting

The system uses a 64-electrode cap with an electrode position of the international standard 10-20 system. There are 6 channels are selected, that is Fp1, Fp2, F3, F4, F7 and F8, in order to match the position of the electrodes in brain death determination. A1 or A2 is the reference electrode as well as the Fz is the ground electrode. The sampling rate is set to 256Hz. The bandwidth is set to 0-60Hz with 50Hz power frequency interference eliminated. The impedance of the electrode is ensured below $10K\Omega$ during the experiment.

4.3.2 Experiment Base on Online Calibration Signal

The g.USBamp device provides a programming API (application programming interface) for Matlab, which can generate online the sinusoidal signal in calibration mode. Therefore the experiment is conducted based on the calibration signal to test the feasibility of system. According to the procedures in figure 4.3, the recording time per cycle is set to 5s, and the number of cycle is set to 2. And the Dynamic ApEn algorithm is selected to analyze online recording data, which is the algorithm to reflect the dynamic complexity change of signals [45]. The experiment is conducted for 10 times.

Figure 4.4 shows 10s with 2 cycles signals are recorded. As can be seen from the figure, there is a case where data is distorted at the beginning of data recording due to the startup of the device. For this case, the distortion is attenuated by increasing the recording time per cycle while reducing the number of cycles. Figure 4.5 shows the analysis results of the signals.

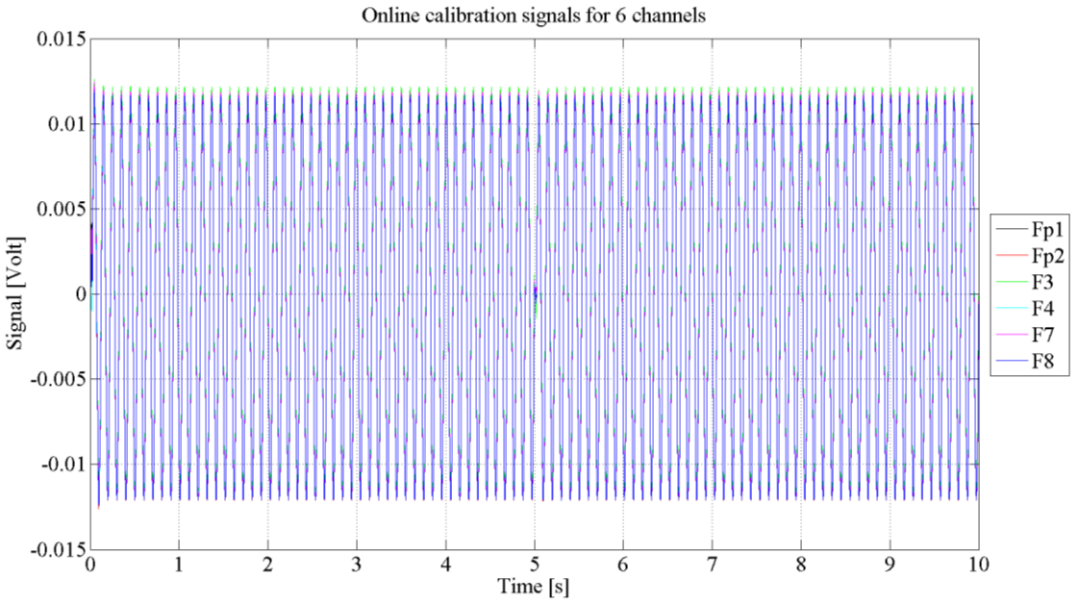

Fig. 4.4 Online calibration signals for one experiment.

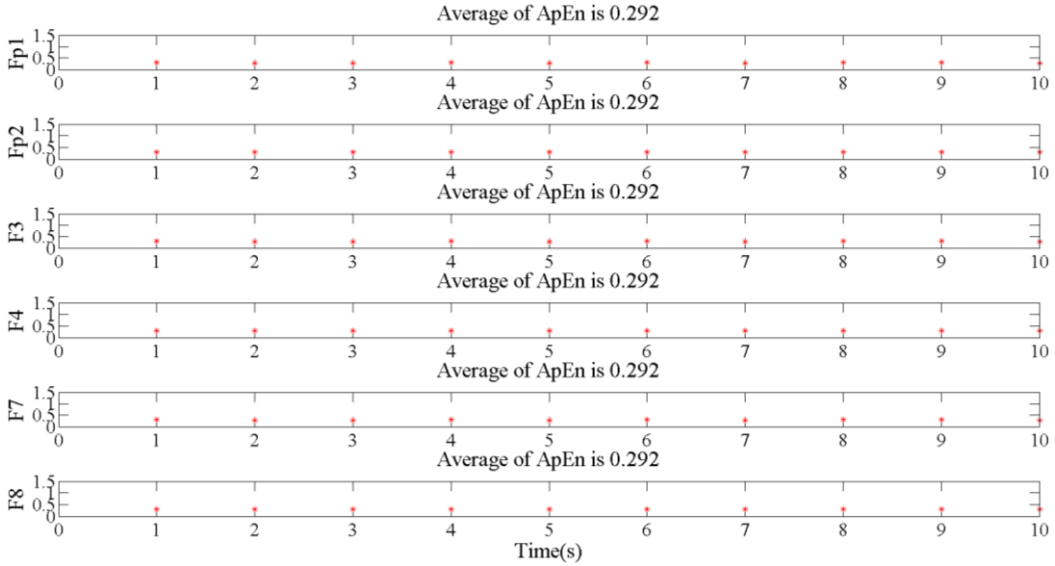

Fig. 4.5 Online analysis results of online calibration signals for one experiment.

Hereafter, the results of 10 experiments were summarized and plot in figure 4.6. From this figure, it is illustrated that results of experiments for 10 times for the same type of online calibration signals are almost the same, which denotes the feasible of online EEG diagnostic system.

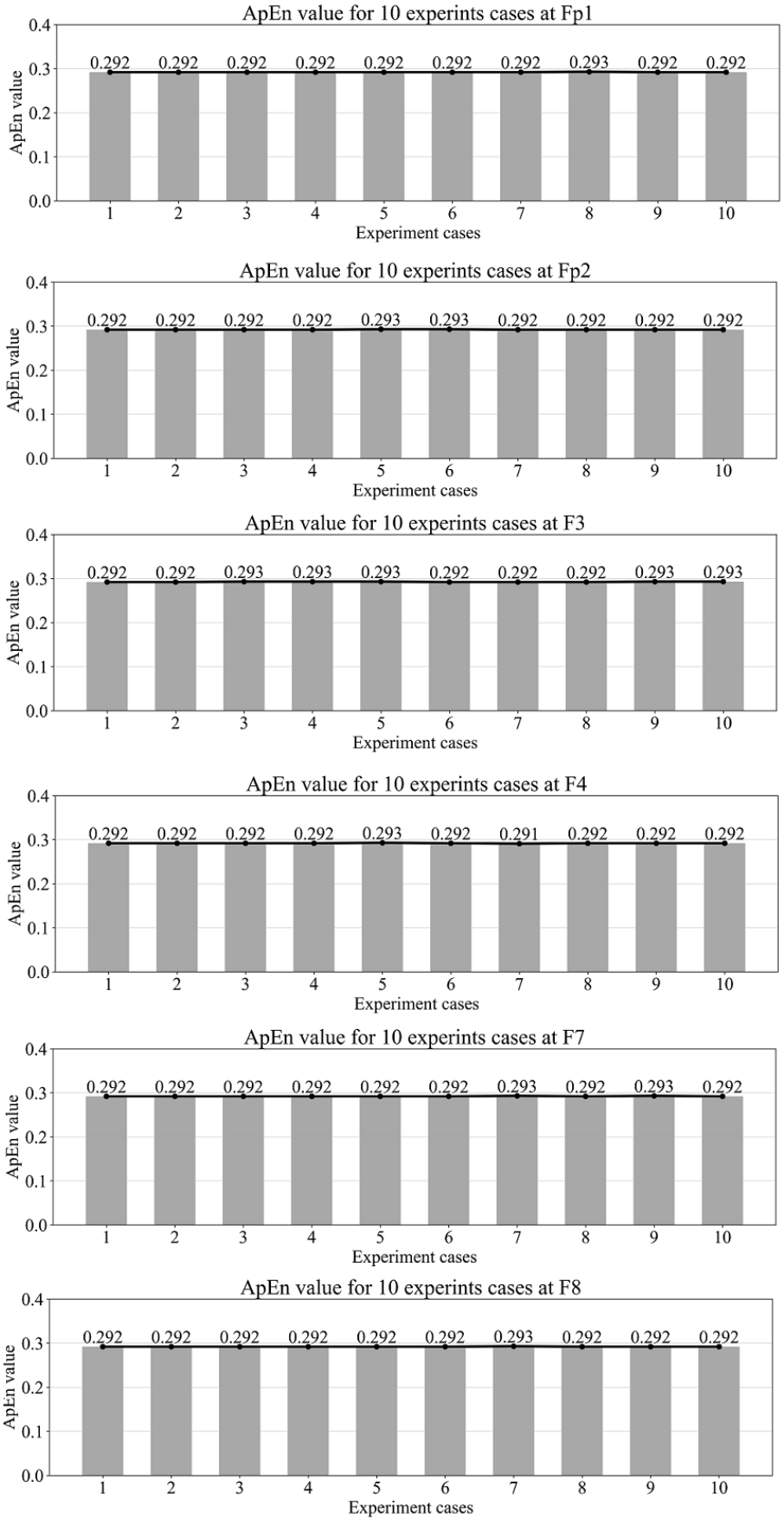

Fig. 4.6 Online analysis results of calibration signals for 10 experiments at 6 channels.

4.4 Chapter Summary

This chapter proposes online EEG diagnostic system. It mainly describes the composition and framework of the system, as well as the experiment based on online calibration signals. Experiment results shows that the system can realize online signals recording and online analysis based on existing algorithms and calibration signals. Moreover, the system includes the alarm function when the analysis results higher than the preset thresholds.

Chapter 5 Conclusions and Future Work

5.1 Conclusions

In this thesis, we study on patients' EEG analysis and realization of online diagnostic system. Specifically, we mainly focus on coma and brain-death patients' EEG as well as epilepsy patients' EEG.

For coma and brain-death patients' EEG analysis, three static EMD-based algorithms were compared from principle and experiments based on standard artificial signals and patients' EEG, and results showed that the 2T-EMD was the algorithm of EEG energy feature extraction with optimal performance. Hereafter, the Dynamic 2T-EMD was proposed and applied to analyze 36 cases of coma and brain-death patients' EEG. Results after processing by descriptive statistics showed that there exists obvious difference of EEG energy between coma patients' EEG and brain-death patients' EEG.

For epilepsy patients' EEG analysis, five method of evaluating PAC strength were used to compute PAC strength of seizure activity and seizure-free intervals at 9 frequency bands based on Bonn dataset. And features were classified by SVM. Moreover, phase-amplitude comodulogram based on the five methods of computing PAC were applied to the same dataset. Results showed that the classification accuracy at $\theta - \gamma$ band was up to 0.96 for seizure detection within epileptogenic zone. And the results were verified intuitively by the phase-amplitude comodulogram.

For the realization of online EEG diagnostic system, the online EEG diagnostic system was consists of one EEG recording device and one laptop, and realized online recording and online analysis based on new developed algorithm. Moreover, this system included an automatic alarm function, in which the system alarmed when the analysis result was above a preset threshold.

5.2 Future Work

For coma and brain-death patients' EEG analysis, more algorithms will be developed and machine learning methods will be used to classify EEG in coma state and EEG in brain-death state based on existed features.

For epilepsy EEG analysis, the performance of filter will be improved. Parameters of classifier will be optimized to increase the classification accuracy. And more real-data will be added to analyze phase amplitude coupling between low frequency phase and high frequency amplitude.

For the realization of online diagnostic system, the interactivity and stability of the system is optimized. And friendly user interface will be designed.

5.3 Chapter Summary

In this chapter, contents of this thesis are summarized. And the future work based on current work is illustrated.

References

[1] Mollaret, P., and M. Goulon. “The depassed coma (preliminary memoir)”, *Revue Neurologique*, vol. 101, no. 101, pp. 3-15, 1959.

[2] Zhonghua Klaus Chen. “Brain-Death—Modern Thanatology”, *Beijing: China Science Publishing*, pp32-33, 2004.

[3] Q.Shi, J. Cao, T. Tanaka, R. Wang, and H. Zhu. “EEG data analysis based on EMD for coma and quasi-brain-death patient”, *Journal of Experimental and Theoretical Artificial Intelligence*, Taylor, Francis, vol. 23, no. 1, pp. 97-110, March, 2011, doi: 10.1080/0952813X.2010.506289.

[4] Scott JB, Gentile MA, Bennett SN, Couture M, Maclntyre NR, “Apnea testing during brain death assessment: a review of clinical practice and published literature”, *Respire Care*, vol. 58, no. 3, pp. 532–538, March, 2013, doi: 10.4187/respcare.01962.

[5] Cao JT, “Analysis of the quasi-brain-death EEG data based on a robust ICA approach”, *Lecture Notes in Artificial Intelligence* Springer-Verlag, vol. 4253, no. 3, pp. 1240-1247, 2006, doi: 10.1007/11893011_157.

[6] Q. Shi, J. Cao, T. Tanaka, R. Wang, and H. Zhu, “EEG data analysis based on EMD for coma and quasi-brain-death patient”, *Journal of Experimental and Theoretical Artificial Intelligence*, vol. 23, no. 1, pp. 97-110, 2011, doi: 10.1080/0952813X.2010.506289.

[7] Y. Yin, J. Cao, Q. Shi, D. P. Mandic, T. Tanaka and R. Wang, “Analyzing the EEG energy of quasi brain death using MEMD”, *Proceedings of the Asia-Pacific Signal and Information Processing Association Annual Summit and Conference*, 2011.

[8] Cui G., et al., “EEG energy analysis for evaluating consciousness level using dynamic MEMD”, *International Joint Conference on Neural Networks* IEEE, 2014, doi: 10.1109/IJCNN.2014.6889716.

[9] Fisher, R. S., et al., “ILAE official report: a practical clinical definition of epilepsy”, *Epilepsia*, vol. 55, no. 4, pp. 475-482, 2014, doi: 10.1111/epi.12550.

[10] Sirven, J. I., “Epilepsy: A Spectrum Disorder”, *Cold Spring Harbor Perspectives in Medicine*, vol. 5, no. 9, 2015, doi:10.1101/cshperspect.a022848.

[11] World Health Organization. Epilepsy. http://www.who.int/mediacentre/factsheets/fs999/en/. (updated February 2018, accessed November 2018)

[12] Assi, Elie Bou, et al., “Towards accurate prediction of epileptic seizures: A review”, *Biomedical Signal Processing & Control*, vol. 34, pp. 144-157, 2017, doi: 10.1016/j.bspc.2017.02.001.

[13] R. Mameniškienė, I. Karmonaitė, and R. Zagorskis, “The burden of headache in people with epilepsy”, *Seizure*, vol. 41, pp. 120-126, 2016, doi: 10.1016/j.seizure.2016.07.018

[14] Jr Engel J., “Early Identification of Refractory Epilepsy”, N Engl J Med, vol. 342, no. 5, pp. 314-319, 2009, doi: 10.1056/NEJM200002033420503.

[15] Ivesdeliperi, Victoria, and J. T. Butler, “Quality of life one year after epilepsy surgery”, *Epilepsy & Behavior E & B*, vol. 75, 2017, doi: 10.1016/j.yebeh.2017.08.014.

[16] Jerome Engel, et al., “Early Surgical Therapy for Drug-Resistant Temporal Lobe Epilepsy: A Randomized Trial”, *The Journal of the American Medical Association*, vol. 307, no. 9, pp. 922-930, 2012, doi: 10.1001/jama.2012.220.

[17] Epilepsy Society. https://www.epilepsysociety.org.uk/. (accessed November 2018)

[18] José F. TéllezZenteno, et al., “Surgical outcomes in lesional and non-lesional epilepsy: A systematic review and meta-analysis”, *Epilepsy Research*, vol. 89, no. 2, pp. 310-318, 2010, doi: 10.1016/j.eplepsyres.2010.02.007.

[19] Adil Harroud, et al., “Temporal Lobe Epilepsy Surgery Failures: A Review”, *Epilepsy Research & Treatmen*t, vol. 2012, 2012, doi: 10.1155/2012/201651.

[20] Jaseja, Harinder, and B. Jaseja, “EEG spike versus EEG sharp wave: Differential clinical significance in epilepsy”, *Epilepsy & Behavior*, vol. 25, no. 1, pp. 137, 2012, doi: 10.1016/j.yebeh.2012.05.023.

[21] Mariano A. Belluscio, et al., “Cross-Frequency Phase–Phase Coupling between Theta and Gamma Oscillations in the Hippocampus”, *Journal of Neuroscience the Official Journal of the Society for Neuroscience*, vol. 32, no. 2, pp. 423, 2012, doi: 10.1523/JNEUROSCI.4122-11.2012.

[22] Alekseichuk I, et al., “Spatial Working Memory in Humans Depends on Theta and High Gamma Synchronization in the Prefrontal Cortex”, *Current Biology*, vol. 26, no. 12, pp. 1513-1521, 2016, doi: 10.1016/j.cub.2016.04.035.

[23] Ibrahim G. M., et al., “Dynamic modulation of epileptic high frequency oscillations by the phase of slower cortical rhythms”, *Experimental Neurology*, vol. 251, no. 2, pp. 30-38, 2014, doi: 10.1016/j.expneurol.2013.10.019.

[24] Guirgis, Mirna, et al., “Defining regions of interest using cross-frequency coupling in extratemporal lobe epilepsy patients”, *Journal of Neural Engineering*, vol. 12, no. 2, 2015, doi: 10.1088/1741-2560/12/2/026011.

[25] Mina Amiri, B. Frauscher, and J. Gotman, “Phase-Amplitude Coupling Is Elevated in Deep Sleep and in the Onset Zone of Focal Epileptic Seizures”, *Frontiers in Human Neuroscience*, vol. 10, no. 59, 2016, doi:

0.3389/fnhum.2016.00387.

[26] Chunsheng Li, et al, “Epileptogenic Source Imaging Using Cross-Frequency Coupled Signals From Scalp EEG”, *IEEE Trans Biomed Eng*, vol. 63, no. 12, pp. 2607-2618, 2016, doi: 10.1109/TBME.2016.2613936.

[27] Cao J., Chen Z., “Advanced EEG signal processing in brain death diagnosis”, *Advanced EEG Signal Processing in Brain Death Diagnosis*. Springer US, pp. 275-298, 2008, doi: 10.1007/978-0-387-74367-7_15.

[28] Huang, N. E., Z. Shen, S. R. Long, M. C. Wu, H. H. Shih, Q. Zheng, N. C. Yen, C. C. Tung, and H. H. Liu, “The empirical mode decomposition and Hilbert spectrum for non-linear and non-stationary time series analysis”, *Proceedings A*, vol. 454, no. 1971, pp.903–995, 1998, doi: 10.1098/rspa.1998.0193.

[29]Rehman N, Mandic D P., “Multivariate empirical mode decomposition”, *Proceedings of the Royal Society A: Mathematical, Physical and Engineering Scienc*es, vol. 466, no. 2117, pp.1291-1302, 2010, doi: 10.1098/rspa.2009.0502.

[30]Julien Fleureau, Jean-Claude Nunes, Amar Kachenoura, Laurent Albera, and Lotfi Senhadji, “Turning Tangent Empirical Mode Decomposition: A Framework for Mono- and Multivariate Signals”, *IEEE Transaction on Signal Processing*, vol. 59, no. 3, pp. 1309-1316, March. 2011, doi: 10.1109/TSP.2010.2097254.

[31] Julien Fleureaua, Amar Kachenouraa, Laurent Alberaa, Jean-Claude Nunesa, Lotfi Senhadjia, “Multivariate empirical mode decomposition and application to multichannel filtering”, *Signal Processing*, vol. 91, no. 12, pp. 2783–2792, December, 2011, doi: 10.1016/j.sigpro.2011.01.018.

[32] Yao Miao, Dongsheng Wang, Gaochao Cui, Li Zhu and Jianting Cao, “Analyzing patients’ EEG energy for brain death determination based on Dynamic 2T-EMD,”

International Journal of Computers & Technology, ISSN 2277-3061, Vol. 16, No. 1, pp. 717-720, DOI: 10.24297/ijct.v16i1.5934, March 2017. (Journal paper)

[33] Yao Miao and Jianting Cao, "Comparison of EMD, MEMD and 2T-EMD by analyzing standard artificial signals and EEG," *2017 International Joint Conference on Neural Networks*, IEEE press, pp. 1367-1371, Anchorage, AK, USA, DOI: 10.1109/IJCNN.2017.7966012, May 2017.

[34] Mann, Prem S., "Introductory Statistics (2nd ed.)", Wiley, ISBN 0-471-31009-3, 1995.

[35] Yao Miao and Jianting Cao, "Descriptive statistical analysis based on patients' EEG energy in coma and quasi-brain-death state," *International Journal of Computers & Technology*, ISSN 2277-3061, Vol. 17, No. 1, pp. 7140-7145, DOI: https://doi.org/10.24297/ijct.v17i1.7171, March 2018.

[36] Andrzejak, Ralph G, et al., "Indications of nonlinear deterministic and finite-dimensional structures in time series of brain electrical activity: Dependence on recording region and brain state", *Phys Rev E Stat Nonlin Soft Matter Phys*, vol. 64, no. 6, 2001, doi: 10.1103/PhysRevE.64.061907.

[37] Canolty RT, Edwards E, Dalal SS, Soltani M, Nagarajan SS, Kirsch HE, et al., "High gamma power is phase-locked to theta oscillations in human neocortex", *Science*, vol. 313, no. 5793, pp. 1626–1628, 2006, doi: 10.1126/science.1128115.

[38] Vanhatalo, S, et al., "Infraslow oscillations modulate excitability and interictal epileptic activity in the human cortex during sleep", *Proceedings of the National Academy of Sciences of the United States of America*, vol. 101, no. 14, pp. 5053-5057, 2004, doi: . 10.1073/pnas.0305375101.

[39] Cohen MX., "Assessing transient cross-frequency coupling in EEG data. J Neurosci Methods", vol. 168, no. 2, pp. 494–499, 2008, doi:

10.1016/j.jneumeth.2007.10.012.

[40] Mormann, Florian, et al., “Phase/amplitude reset and theta–gamma interaction in the human medial temporal lobe during a continuous word recognition memory task”, *Hippocampus*, vol. 15, no.7, pp. 890-900, 2010, doi: 10.1002/hipo.20117.

[41] W. D. Penny, E. Duzel, K. J. Miller, and J. G. Ojemann, “Testing for nested oscillation”, *Journal of Neuroscience Methods*, vol. 174, no.1, pp. 50-61, 2008, doi: 10.1016/j.jneumeth.2008.06.035.

[42] Tort AB, Komorowski R, Eichenbaum H, Kopell N, “Measuring phase-amplitude coupling between neuronal oscillations of different frequencies”, *Journal of Neurophysiology*, vol. 104, no. 2, pp. 1195-1210, 2010, doi: 10.1152/jn.00106.2010.

[43] Tolga EsatÖzkurt, Alfons Schnitzler, “A critical note on the definition of phase‐amplitude cross-frequency coupling”, *Journal of Neuroscience Methods*, vol. 201, no. 2, pp. 438-443, 2011, doi: 10.1016/j.jneumeth.2011.08.014.

[44] Fawcett T., “An introduction to ROC analysis”, *Pattern Recognition Letters*, vol. 27, no. 8, pp. 861-874, 2005, doi: 10.1016/j.patrec.2005.10.010.

[45] Yao Miao, and J. Cao, “Patients’ EEG Analysis Based on Multi-indicator Dynamic Analysis Measure for Supporting Brain Death Determination”, *International Symposium on Neural Networks* Springer, Cham, vol. 10878, 2018, doi: 10.1007/978-3-319-92537-0_93.